Mineralogy and Petrology (2006) 87: 351–384
DOI 10.1007/s00710-006-0125-9

Mineralogy and Petrology
Printed in Austria

Gold scavenged by bismuth melts: An example from Alpine shear-remobilizates in the Highiş Massif, Romania

C. L. Ciobanu[1], **N. J. Cook**[2], **F. Damian**[3], and **G. Damian**[3]

[1] Department of Earth Sciences, University of Adelaide, Adelaide, Australia and South Australian Museum, Adelaide, Australia
[2] Natural History Museum, University of Oslo, Oslo, Norway
[3] North University of Baia Mare, Baia Mare, Romania

Received April 25, 2005; revised version accepted February 27, 2006
Published online June 6, 2006;
Editorial handling: P. Spry

Summary

Gold mineralization occurs in the Şoimuş Ilii vein, the main Cu prospect in the Highiş Massif, Western Apuseni Mts., Romania. The Highiş Massif is part of the Highiş Biharia Shear Zone, a 320–300 Ma Variscan greenschist belt, with a 114–100 Ma Alpine overprint. In Highiş, phyllonites enclose an igneous core consisting of an Early Permian basic complex intruded by Middle Permian granitoids. The vein is hosted within basalt hornfels at its contact with the 264 Ma Jernova granite. Gold is not only present as native gold, but also as jonassonite (ideally $AuBi_5S_4$). The latter occurs as inclusions 1–30 μm in size in chalcopyrite; microanalysis gives the empirical formulae $Au_{1.02}(Pb_{0.47}Bi_{4.51})_{4.98}S_4$. The two Au minerals are spatially associated with Bi–(Pb) sulfosalts (oversubstituted bismuthinite, cosalite) and sulfotellurides/selenides (ingodite, ikunolite and laitakarite) in blebs/patches, mainly hosted in chalcopyrite. This Au–Bi–Te association overprints an earlier, chalcopyrite-quartz assemblage, occurring as trails along discrete zones of brecciation that crosscut former mineral boundaries. Curvilinear and cuspate boundary textures within the blebs/patches suggest deposition in a molten form. Mineral associations in combination with phase relations indicate that the Au–Bi–Te association formed as a result of melting of pre-existing native Bi (and possibly sulfosalts) at 400 °C under sulfidation conditions. These melts incorporated Au, Pb, Te and S as they moved in the vein during shearing and were locked within dilational sites. Native Bi occurs as coarse aggregates along vein margins, but in the Au–Bi–Te association, it is present only as small droplets in shear gashes, never together with other Bi- and Au-minerals. The Bi-derived melts are part of an internal remobilizate which also includes chlorite and adularia. Minerals in the system Au–Bi–Te

were deposited from a neutral low reducing fluid during Alpine shearing in the Early Cretaceous. The fluid also assisted solid-state mobilisation of chalcopyrite and cobaltite. This study illustrates the significant potential of Bi, a low melting-point chalcophile element (LMCE), to act as Au scavenger at temperatures as low as 400 °C.

Introduction

There is a strong association between shear zones and orogenic Au mineralization because shear zones are thought to act as conduits for Au-bearing metamorphic fluids (e.g., *Groves* et al., 1998). Shear zones have major exploration significance when targeting this type of Au mineralization but there are few known occurrences of orogenic Au in the Alpine shear belts in Europe (*Goldfarb* et al., 2001). In this paper, we present new data for an Au mineralization spatially associated with a Variscan belt that experienced Alpine shearing, the Highiş Biharia Shear Zone (HBSZ) in the Apuseni Mountains, Romania (e.g., *Pană* and *Erdmer*, 1994).

Deformation of a pre-existing ore during metamorphism can affect the primary distribution of metals, on scales ranging from a few mm to several hundreds of meters. Of particular importance is the potential formation of discrete Au-rich parts within a given deposit. Such ores are considered 'remobilizates' since they are generated by remobilization of pre-existing metals or minerals (or both) within an orebody or orefield. Remobilizates are commonly characterized by an unusual or 'exotic' trace mineralogy, in which elements such as As, Ag, Sb, Bi and Te may be prominent. Although solid state diffusion and dissolution-reprecipitation mechanisms have generally been be invoked to explain the formation of remobilizates (e.g., *Marshall* et al., 2000), a third mechanism, involving the generation of sulfide melts, which may carry precious metals, has recently commanded attention (*Frost* et al., 2002). The presence of sulfide melts is possible because a number of low melting-point chalcophile elements (LMCE), including those which often occur in remobilized assemblages, form sulfosalts and chalcogenides with low-melting temperatures. Partial melting of a sulfide ore occurs if it undergoes metamorphism at temperatures above the melting point of some of the available ore minerals. The importance of partial melting of a pre-existing ore is that such melts may act as scavengers for Au, a metal that otherwise has a high melting point (e.g., Challenger, SE Australia; *Tomkins* and *Mavrogenes*, 2002, 2003; Hemlo, Canada; *Tomkins* et al., 2004). The gold need not be concentrated within the ore prior to remobilization, but could be present at low concentrations in the surrounding rocks or even introduced from an external source, and subsequently scavenged by the sulfide melts.

We report new mineralogical data from a vein at Şoimuş Ilii, the main vein prospect in the Highiş Massif (*Giuşcă*, 1957), which is part of the HBSZ. The vein is hosted by basalt hornfels at the contact with a Middle Permian granitoid. The mineralization was considered to be either associated with the host basalt complex (*Giuşcă*, 1957; *Brana*, 1958), or to be granite-related (*Ianovici* et al., 1976). Bismuth minerals, yet no gold minerals, were previously reported from this vein (*Giuşcă*, 1957). The present contribution focuses on presenting the mineralogical and petrological aspects of this occurrence, which are used to support a plausible model of formation. This model will suggest that the Au mineralization formed after the main Cu ore in the vein and was associated with shearing and accompanying metamorphism recorded within

the HBSZ. Our model also involves incorporation of Au within Bi-rich melts that formed during low-grade metamorphism of pre-existing Cu ore within the vein.

Geological setting and previous work

The Highiş Massif forms the southwesternmost edge of the Apuseni Mts. (Romania), an Alpine orogenic unit situated within the Carpathians (Fig. 1a). The Highiş Biharia Shear Zone (Fig. 1b) represents a Variscan greenschist shear zone with Alpine overprint (e.g., *Pană* and *Erdmer*, 1994; *Dallmeyer* et al., 1999; *Pană* et al., 2002). The HBSZ stretches along the boundary between the North and South Apuseni Mts. It thus, runs parallel to the Carpathian orocline and separates two gneissic domains in the Apuseni Mts. (Fig. 1b). A granite-gneiss terrane to the north (Someş) is bounded by an amphibolite/granodiorite belt (Codru), and a mica schist and gneiss terrane hosting lenses of carbonates occurs to the south (Baia de Arieş). These three terranes belong to different tectonic units in the Northern Apuseni Mts., and form a Mid-Cretaceous edifice of several nappe complexes which are from the lower part upwards: the Bihor para-autochthon (Someş), Codru and Biharia (Baia de Arieş) (e.g., *Bleahu* et al., 1981).

The HBSZ is a composite belt in which phyllonites surround igneous cores (Late Cambrian, Biharia; Early-Middle Permian, Highiş), which were preserved as low strain pods during Alpine shearing (*Pană* et al., 2002). The igneous pods (varying from m to km in size) consist of a variety of different rock types, including gabbro, diorite, alkali-granite, syenite, granodiorite and granite, and may also occur outside the cores, within the phyllonites.

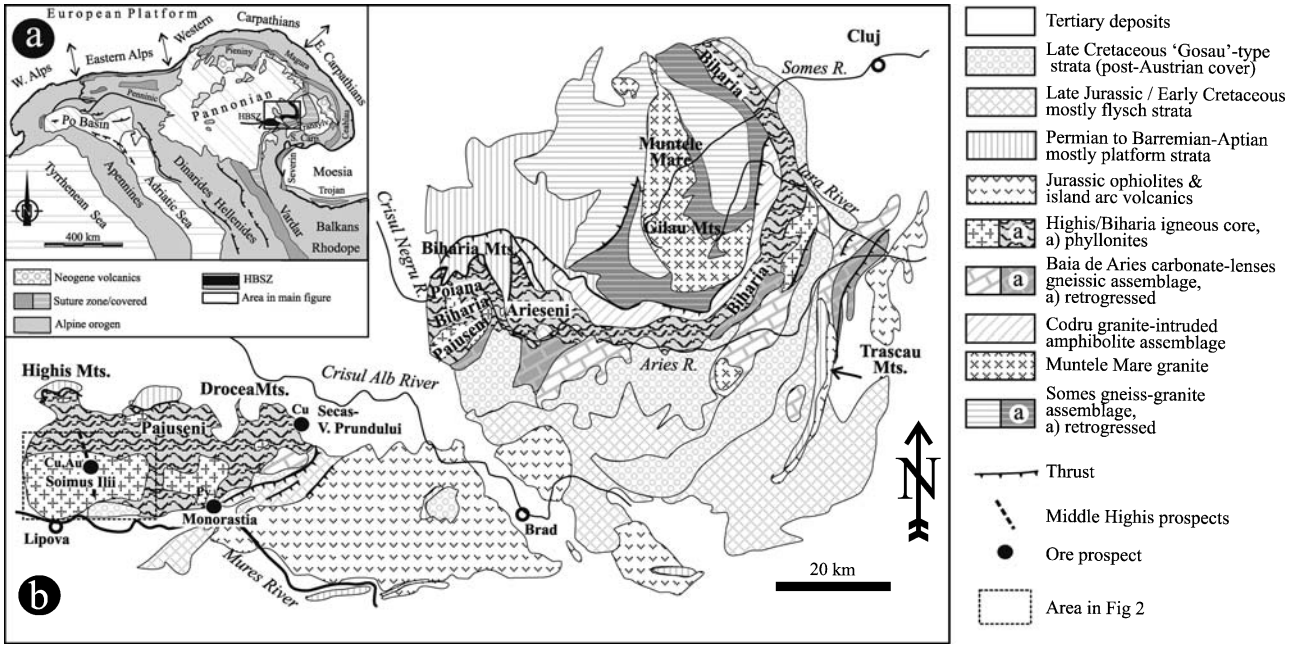

Fig. 1. **a** Location of Apuseni Mountains within the Alpine Orogen. **b** Geological sketch map of the Apuseni Mts., indicating the location of the Highiş Massif and the Highiş-Biharia Shear Zone (after *Dallmeyer* et al., 1999; *Pană* et al., 2002)

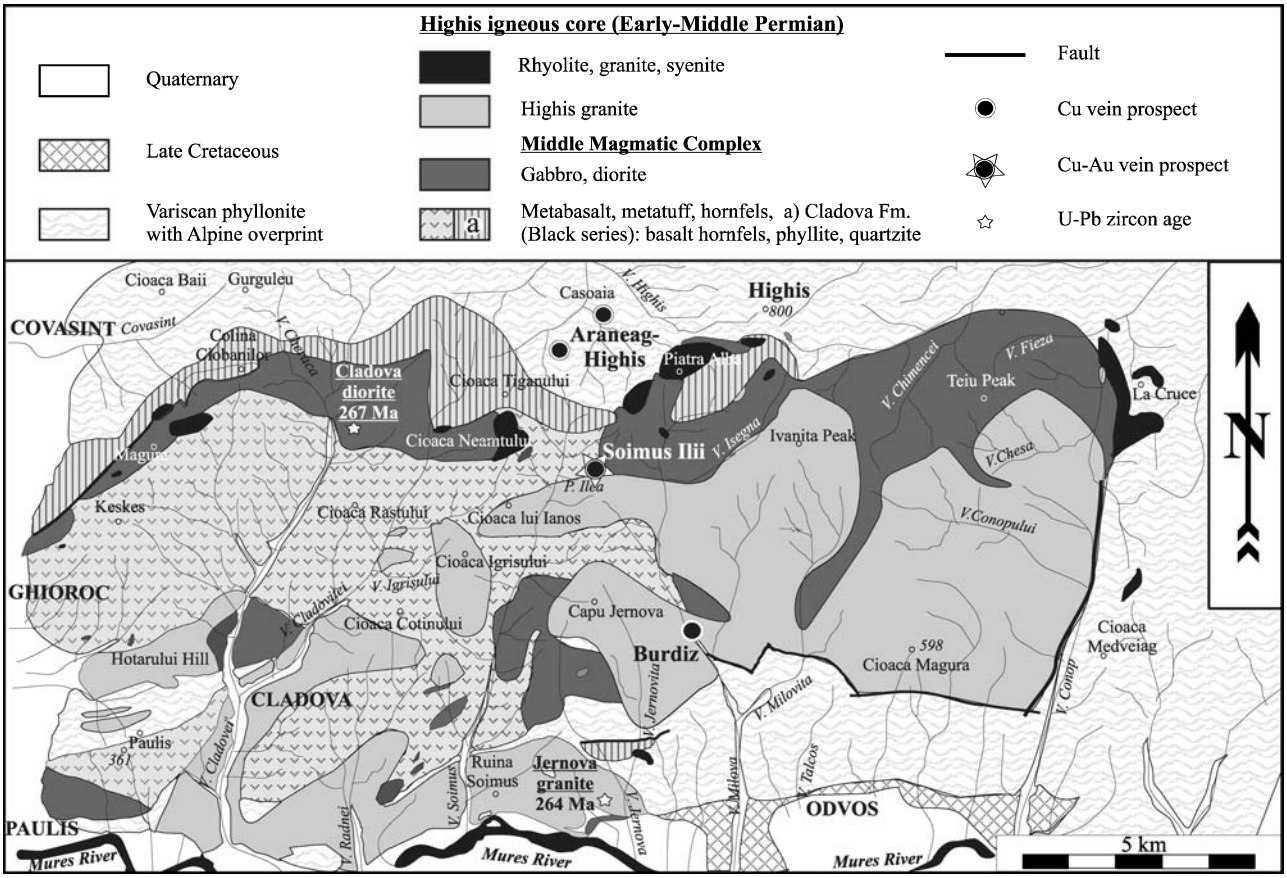

Fig. 2. Geological map of the Highiş Massif showing the location of mineral deposits/prospects (after *Giuşcă*, 1979; modification of legend after *Pană* and *Ricman*, 1988; *Dallmeyer* et al., 1999; *Pană* et al., 2002). U/Pb zircon ages from *Pană* et al. (2002)

Igneous rocks in the Highiş Massif

Igneous rocks which form the core of the Highiş Massif (also including the smaller but similar igneous core in the Drocea Massif) comprise early basic volcanics and plutons ('Middle Magmatic Complex', 'ophiolitic complex') followed by granitic to alkaline intrusions (Fig. 2). The Highiş granitoids were considered as Variscan (Hercynian) synorogenic intrusions (e.g., *Ianovici* et al., 1976), as indicated by a whole-rock K–Ar age of ~350 Ma obtained from granite in the Highiş Mts. (*Giuşcă* et al., 1968). *Pană* et al. (2002) provided more precise zircon U–Pb ages on two intrusions that bracket magmatic activity in the igneous core. They dated the early Cladova diorite body, previously considered a Variscan intrusion (*Balintoni*, 1986) or Caledonian ophiolitic crust (*Dimitrescu*, 1985), and the late Jernova porphyritic microgranite (Fig. 2). Ages of 267 and 264 Ma, respectively, led *Pană* et al. (2002) to conclude that the igneous core belonged to a short-lived magmatic event which formed part of the third magmatic episode in the Apuseni Mts. The event is dated at between 278 (age of the Muntele Mare granite; Fig. 1b) and 264 Ma. Although the presence of a basic volcano-plutonic complex suggests a rift setting

(the 'ophiolitic complex'; e.g., *Ianovici* et al., 1976), geochemical characteristics of the igneous core more closely resemble those of a continental rift rather than an oceanic rift (*Pană*, 1998). Generation of the Early to Middle Permian dioritic and granitic magmatism in the Highiş Massif, and the associated clastic rocks (affected by later metamorphism), is attributed to stretching along a zone that represents a crustal discontinuity between different terranes in the Apuseni Mts. (*Pană* et al., 2002). The igneous cores in both the Highiş and Biharia Massifs were overprinted by the same shearing and retrograde metamorphic events responsible for phyllonite formation within the HBSZ.

Hornfels

Hornfels is formed in the contact aureole of the Highiş and Biharia granitoids. Intrusive contacts along the southern part of the core are also marked by migmatites, which are considered to be evidence for synorogenic emplacement of the granitoids (e.g., *Ianovici* et al., 1976). Biotite is the key mineral in identifying the hornfels associations; amphibole (actinolite) appears only at the contact of the smaller intrusions on the northern side of the core. Here, cordierite hornfels also occur within phyllitic schists of the 'Black series' (*Dimitrescu*, 1962), also known as the 'Cladova Formation' (*Balintoni*, 1986) (Fig. 2). *Dimitrescu* (1962) considered these schists to be a Permian sedimentary cover overthrust by the ophiolite complex, whereas *Balintoni* (1986) considered them to be Carboniferous in age and contact metamorphosed together with the ophiolitic complex. *Pană* and *Ricman* (1988) interpreted them to be basalt hornfels and include the sequence within the Middle Magmatic Complex. The deformation of hornfels spots in the vicinity of the shear planes suggested to *Pană* and *Ricman* (1988) that they were subsequently deformed. In the southern part of the igneous complex, hornfels formed from schists at intrusive, synkinematic contacts at albite-epidote facies (quartz-albite-epidote-muscovite-biotite, encompassing temperatures in the range 300–600 °C) (*Ianovici* et al., 1976).

The phyllonites

The protolith of the phyllonites is uncertain, although they appear, at least partially, to be derived from igneous rocks. This interpretation is based upon evidence that shows a progressive transition from igneous to phyllonite textures at the contact between the two rock types, as observed in the northern part of the Highiş Mts. (*Pană* and *Ricman*, 1988). Moreover, a partial compositional overlap between the igneous pods and their phyllonitic matrix suggests formation of the latter by shearing and metasomatism of a granite protolith. *Dallmeyer* et al. (1999) considered that all assemblages within the HBSZ mentioned earlier are derived from mafic-felsic subvolcanic sequences and gabbro-diorite-granite tectonic enclaves that underwent shearing. This is in contrast to previous work that considers sedimentary and igneous rocks to be the pre-metamorphic protoliths in most of the lithological units under discussion (e.g., *Ianovici* et al., 1976). One such example is the 'Formaţiunea detritogenă' of *Giuşcă* (1962, 1979) in the Highiş Massif, which comprises metamorphosed conglomerates, sandstones, and greywackes. Based

upon εNd values and calculated T_{DM} of representative lithotypes in the HBSZ, *Pană* et al. (2002) acknowledge, as an alternative to the metasomatic model, that some of the quartz-clast-bearing mylonitic schists (based on a sample from Highiş) may represent a sheared Paleozoic conglomerate.

Conditions of metamorphism

The debate concerning the origin of the Highiş Massif allows the metamorphic reactions that led to formation of greenschist facies rocks within the HBSZ to be determined, particularly the phyllonites in the Highiş Massif. *Giuşcă* (1962, 1979) considered prograde metamorphic reactions for rocks they interpreted to be sedimentary in origin, while *Pană* and *Ricman* (1988) discussed retrograde metamorphic reactions since they considered the precursor rocks to be igneous. *Pană* and *Erdmer* (1994) also considered most of the rocks in the entire HBSZ to be igneous. These authors provided a general evaluation of the metamorphic conditions for greenschist belts within the Apuseni Mts. and Romanian Carpathians, which is also applicable to the HBSZ. They proposed that shearing was accompanied by an influx of fluids that produced an alteration assemblage (chlorite + epidote + actinolite + albite + white mica + magnetite + quartz) developed symmetrical to the shear zone axis. The presence of lenses rich in quartz, carbonate and graphite, with a probable metasomatic origin, accounts for the extent of greenschist facies re-equilibration. Mineral assemblages in the axial plane indicate metamorphic conditions >400 °C, while re-equilibration temperatures may be as low as 280–250 °C (calcite-dolomite geothermometry in carbonate lenses from HBSZ; *Pană*, unpubl. data, cited in *Pană* and *Erdmer*, 1994). No independent pressure estimates are available for the HBSZ.

Age of shearing

The age of the first shearing episode within the HBSZ is loosely constrained by the local presence of Permian (?)-Triassic sedimentary cover that is not affected by metamorphism (*Pană* and *Erdmer*, 1994). *Dallmeyer* et al. (1999) presented $^{40}Ar/^{39}Ar$ data from muscovite and whole rocks in a suite of nine samples of variably deformed rocks along the HBSZ. Collectively, the results indicate a moderate thermal event (ca. 300–350 °C) at 320–300 Ma (Late Carboniferous), followed by a second thermal episode (ca. 150–100 °C) at 114–100 Ma (Albian to Aptian). We note that the above temperature ranges appear to be lower than those given by *Pană* and *Erdmer* (1994). This can be explained by the fact that only three samples, all restricted to the northern margin of the shear zone, were examined (i.e., from the NW edge across the phyllonites between the sedimentary cover to the north and the igneous core to the south). Hence, the above temperatures ranges are not representative for the median part of the shear zone in which the Şoimuş Ilii deposit is located.

Thrusting and shearing during the later event, in the Early to Mid Cretaceous, was also accompanied by low-grade metamorphism. Available data for the Apuseni Mts. do not indicate a Cenozoic (Late Alpine) overprint following the Mesozoic (Early Alpine) event, as has been encountered in other low-grade ductile shear zones from the Internal Alps and Carpathians (*Dallmeyer* et al., 1999).

Mineralization

The Late Alpine event mentioned above also has metallogenetic significance, in that orogenic Au mineralization is known from several localities in the Austrian, Italian and Swiss Alps (*Goldfarb* et al., 2001). The Eastern Alps of Austria feature Au deposits of Alpine age characterized by the presence of Bi-minerals (e.g., *Horner* et al., 1997). In contrast, only Cu mineralization has been reported previously within the HBSZ. The most significant mineralization is a Cu district in the middle of the Highiş Massif that comprises several Cu vein prospects, either within the igneous core (e.g., Şoimuş Ilii, and at Burdiz, Milova Valley) or in the phyllonites from the northern part of the massif (Arăneag – Valea Highiş, Fig. 2). Other prospects include a phyllonite-hosted Cu district at Secaş – Valea Prundului and an area with pyrite mineralization at Monorăştia, which is located at the eastern edge of the Drocea Massif, and at the southern margin of the granite in the Drocea Massif, respectively (Fig. 1b). Although the mineralization is hosted either within or outside the igneous core, it is currently considered to be granite-related (e.g., *Ianovici* et al., 1976), even though not all authors agree with this point of view (see below). The Şoimuş Ilii prospect was explored in the late 1950's, on the site of small-scale mining before the First World War. Other copper deposits in the Milova Valley to the south had been worked in medieval times (*Brana*, 1958).

In the Highiş district, the ore comprises chiefly chalcopyrite and pyrite in quartz veins; bornite also occurs in the phyllonite-hosted veins. The mineralized quartz veins are located along fractures with a general E–W and/or WNW–ESE trend, concordant with the rock foliation. Strong lamination and shearing of the host rocks are also noted. The prospects occur along a NNW–SSE trend that is probably associated with a shear zone, which cross-cuts the general E–W strike of the main shear zone (Fig. 2). This interpretation is also supported by the observation that in the phyllonites on the northern side of the alignment (Highiş basin), there is an open E–W antiform (*Pană* and *Ricman*, 1988).

The Burdiz and Şoimuş Ilii vein prospects have been extensively explored in the Highiş Massif. Several smaller showings are also known within the Milova and Şoimuş valleys (*Ianovici* et al., 1976). The Burdiz prospect is located within the sheared 264 Ma Jernova granite (part of Highiş Massif), whereas the Şoimuş Ilii prospect is hosted within the basalt hornfels formed at the northern contact with the same body, some 4 km to the NNW. Even though the two main veins within these prospects share characteristics, such as the lens-like morphology with widely variable width (0.05 to 1 and 1.5 m) and comparable E–W strikes and steep dip to the south, the Şoimuş Ilii prospect is at least twice as long and deep (explored along a length of 800 m at upper levels and 500 m at levels down to 90 m) than the Burdiz prospect (length 190 m, to a depth of 43 m). *Brana* (1958) quotes grades of 1–2% Cu for the Şoimuş Ilii prospect.

The main mass of the Şoimuş Ilii vein is quartz, but unlike the other veins, this vein also contains disseminated apatite. *Giuşcă* (1957) noted the high concentration of massive cm-sized aggregates of apatite in the vein; small quantities of siderite are also present. Apart from the main ore minerals (chalcopyrite and pyrite), sphalerite and marcasite are also noted in minor or trace amounts.

Giuşcă (1957) reported a compact aggregate (up to 1 cm in width) at the margin of the Şoimuş Ilii vein with a distinct mineralogy relative to the main ore assem-

blage. It consists mainly of glaucodot, [(Co,Fe,Ni)AsS], cobaltite (CoAsS), and native Bi and minor chalcopyrite, galena, tennantite [$(Cu,Fe)_{12}As_4S_{13}$] and cubanite ($CuFe_2S_3$). Galenobismutite ($PbBi_2S_4$) was also mentioned, but had been identified, like all the minerals mentioned above, by optical methods only. Because of these mineralogical characteristics, *Giuşcă* (1957) concluded that the mineralization at the Şoimuş Ilii prospect represents a 'Cu ± Co, Bi association' with quartz, carbonate and apatite gangue, of 'hypo- to mesothermal' type, affiliated to 'the Cu-chlorite formation' of *Schneiderhöhn* (1941). This type of mineralization is generally located in basic rocks, and *Giuşcă* (1957) accordingly associated the vein formation with an early basic (diorite?) intrusion which may be part of the host basaltic complex rather than the later granite; *Brana* (1958) agreed with this opinion. *Ianovici* et al. (1976) considered this a misinterpretation of the aforementioned classification scheme since *Schneiderhöhn* (1941) himself discusses a granite-related genesis for this type of association. The granite-related affiliation of the Cu mineralization throughout the Highiş Massif was also endorsed by *Savu* and *Kräutner* (1972).

Petrography and textures of mineral assemblages in the vein

Sulfide and gangue minerals

In the present samples (from the mine dump at the Şoimuş Ilii prospect), the main sulfides are chalcopyrite and pyrite; cobaltite is the most widespread minor com-

Fig. 3. Back-scattered electron images showing textural aspects of minerals in the vein. **a** Cobaltite with two zonation trends: (i) Fe-free margins grown onto resorbed core, (ii) fracture-induced chaotic disturbance at the margin where corrosion is present. **b** Pyrite-magnetite symplectites formed by replacement of pyrrhotite. **c** Clot of apatite with interspersed quartz, chalcopyrite and epidote. **d** Brecciated grain of REE-bearing epidote situated along a shear, i.e., adularia formed between the corner of epidote and albite. Note the subtle zonation in epidote given by variation in REE content and the low-REE overgrowth. **e** Dusty monazite inclusions (white) in the core (marked) of a deformed apatite grain. **f** Brecciated REE-carbonate (parisite?). **g** Retrograde chlorite after biotite. Note also the shearing in quartz. **h**, **i** Zonation, due to variation in $Mg/(Mg + Fe)$, in chlorite interpreted to replace an amphibole from the hornfels. In *i* Turbid Mg-rich areas in host chlorite surround albite which is deformed during shearing. **j** Shear-oriented zonation trends in new-formed (hydrothermal) chlorite (Mg-rich cores). **k** Growth-induced cracks (arrowed) surrounding chlorite within chalcopyrite. Note the absence of cracks around the nearby biotite and muscovite. **l** Clot of feldspars at the boundary between chalcopyrite and quartz. **m** Granoblastic texture in quartz. **n** Embayment between deformed pyrite and quartz. Note the radial arrangement of quartz around the pyrite knot (arrowed), indicating that deformation was subsequent to the formation of the two minerals. **o** Caries boundary between soft and hard minerals (chalcopyrite, cobaltite, apatite and quartz). Note the shearing fractures in chalcopyrite and apatite (arrow). Abbreviations: Ab – albite, Adu – adularia, Ap – apatite, Bt – biotite, Chl – chlorite, Cob – cobaltite, Cp – chalcopyrite, Ep – epidote, Kfs – K-feldspar, Mu – muscovite, Par – parisite, Py-Mt – pyrite-magnetite, Qz – quartz, REE-Ap – REE-bearing apatite, Ru – rutile. All scale bars: 50 μm (except n: 500 μm)

ponent. Much of the cobaltite is found as isolate grains or skeletal clusters within chalcopyrite. Compositional zonation patterns, expressed as variable amounts of Fe (4–11 wt.%; see below) are typical for cobaltite in the deposit. Although these patterns are in most cases chaotic, their appearance in some larger grains is, at least partially, the result of two overlapping trends. As shown in Fig. 3a, primary zonation is represented by a resorbed core surrounded by Fe-poor margins. The cause of the chaotic compositional variation is related to the fractures seen at the

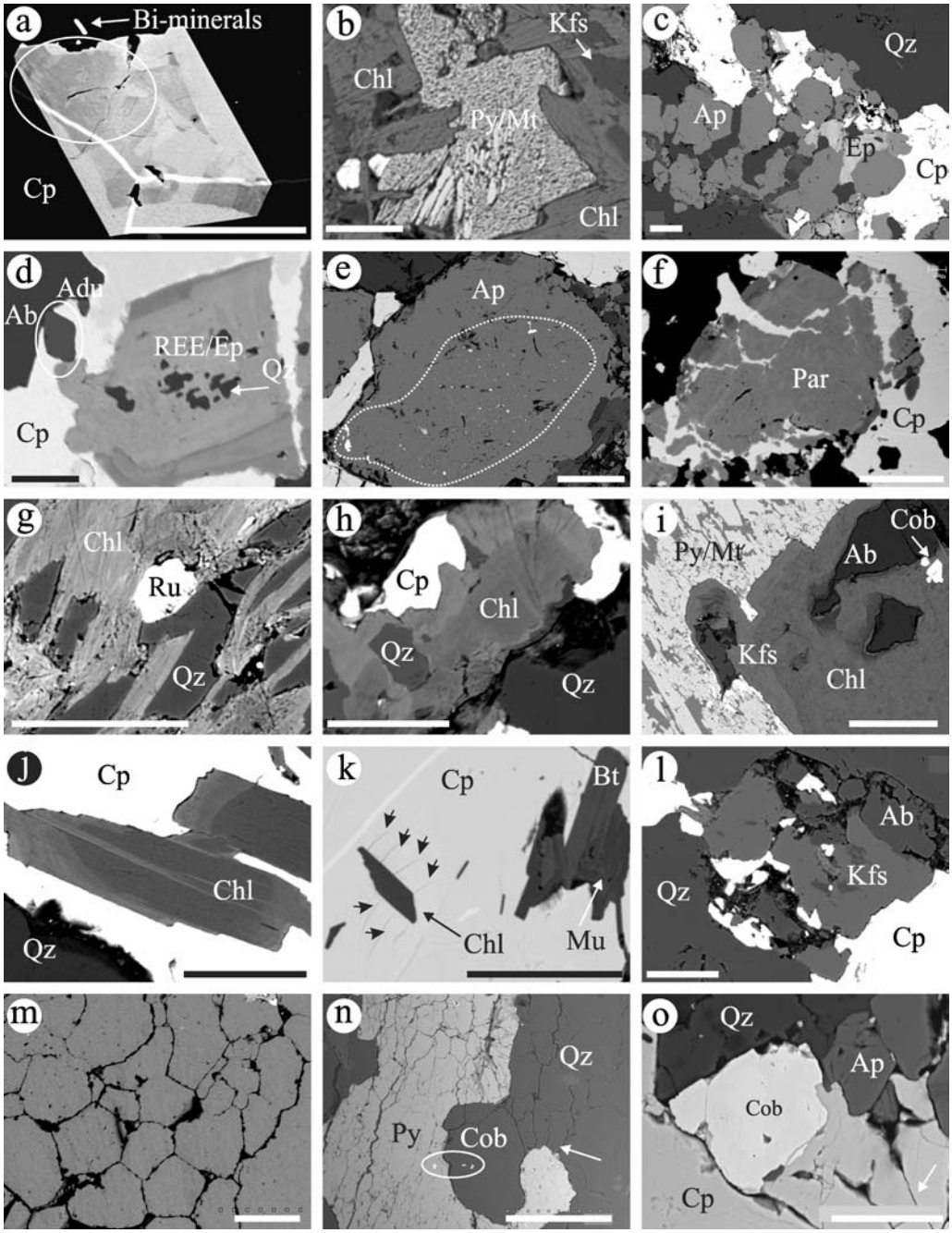

grain boundary, which exhibits marginal corrosion. Pyrite is persistently marked by the presence of relict pyrrhotite as cores. Pyrite formation from pre-existing pyrrhotite is also indicated by replacement textures consisting of symplectitic pyrite-magnetite intergrowths (Fig. 3b). Pyrrhotite is also observed as inclusions in chalcopyrite; some of these contain exsolutions of pentlandite [$(Ni,Fe)_9S_8$]. Sphalerite is rare but is locally present as disparate skeletal bodies within chalcopyrite.

Quartz is the main gangue mineral (60 vol.% of gangue). Apatite is the second most abundant vein component (20 vol.%), occurring either as disparate grains or forming mm-size clots. The larger aggregates of apatite are interspersed with chalcopyrite, quartz, and to a lesser extent, epidote (Fig. 3c). Epidote, a minor yet widespread vein mineral, shows REE-enrichment towards allanite-(Ce). Cores of epidote can have Ce contents as high as 6.5 wt.% Ce_2O_3 (Fig. 3d). Compositional zoning in epidote is defined by slight variations in the REE content across the grain. The REE-rich signature of the vein is also due to the presence of monazite-(Ce) [$(Ce,La,Nd,Th)PO_4$], and a REE-carbonate [parisite? – $Ca(Ce,La)_2(CO_3)_3F_2$; Fig. 3e, f]. As shown in Fig. 3e, a large apatite grain has a core with fine inclusions of monazite. Such inclusions can contain as much as 66 wt.% REE_2O_3 (29 wt.% Ce_2O_3, 29 wt.% Nd_2O_3, 8 wt.% La_2O_3).

Minerals of metamorphic and/or hydrothermal origin

Taking the metamorphic quartz-albite-epidote-muscovite-biotite ± actinolite vein assemblage resulting from the Middle Permian contact metamorphic event as a starting point, we document the mineralogical and petrographic changes resulting from Alpine shearing that are associated with an influx of hydrothermal fluids. Several minerals are unmodified, apart from being brecciated or fractured, but other minor minerals within the vein are useful for understanding the petrogenetic history of the ore. These minerals include chlorite [$(Mg_{5.7–2.5}Fe_{2.7–5.8}Al_{3.3})_{11.6}(Si_{5.5}Al_{2.5})_8O_{28}$], biotite, muscovite, K-feldspar ($Kfs_{97}Ab_3$), albite ($Ab_{98}An_2$), zircon, rutile and titanite. Most abundant is chlorite (Fig. 3g) and much of it has replaced biotite and/or actinolite (Fig. 3h). Although no actinolite relicts were noted, variable Mg/(Mg + Fe) trends in chlorite could be inherited from precursor actinolite in the hornfels rather than biotite. Compositional zoning in chlorite can also be seen in former actinolite-feldspar assemblages that were replaced during a shearing event, with zonation patterns preserved in pressure shadows surrounding the more refractory components of the assemblage (Fig. 3i). Compositional zoning is also recognized in new-formed chlorite, which is also formed during the shearing event (Fig. 3j). Larger masses of altered biotite and actinolite (or both) are associated with feldspar and are found as discontinuous bands or clots within the quartzitic mass of the vein. These assemblages most probably represent fragments of the basalt hornfels that were incorporated in the vein as it formed.

Some muscovite, biotite, chlorite and feldspar appear, however, to have formed directly from the hydrothermal fluid(s) at the time of ore deposition. For example, small flakes of biotite, muscovite and chlorite are found in chalcopyrite, but only chlorite is observed within growth-induced penetrative cracks (Fig. 3k). This implies that even though these minerals coexist with chalcopyrite, their formation is contemporaneous with chalcopyrite growth in the case of biotite and muscovite

but subsequent to the host in the case of chlorite. Biotite is green and has the following composition [$(K_{1.5}(Mg_{3.2}Fe_{1.5}Al_{1.1})_{5.8}(Si_{5.7}Al_{2.3})_8O_{22}$]. Chlorite is also Mg-rich [$Mg/(Mg + Fe) = 0.68$]. Some feldspar within chalcopyrite, at the boundary between sulfide and larger bodies of quartz (Fig. 3l), may also be associated with ore deposition from hydrothermal fluid rather than from inherited fragments of hornfels. Certainly, the small adularia grain at the tip of epidote in Fig. 3d has a hydrothermal origin. Chalcopyrite appears to have been remobilized along fractures within the nearby silicates.

Zircon and Ti-minerals are widespread within the retrogressed hornfels assemblages. These minerals also show evidence of an inherited history in their primary zoning patterns, which were subsequently sheared and brecciated, and overgrown by hydrothermal grains. Titanite is more abundant than rutile; the latter also shows relicts of ilmenite.

Ore textures

Chalcopyrite and pyrite occur as mm- to cm-scale, aligned lenses and nests that parallel the margin of the vein. A second fabric, oblique to this orientation, is recognizable in the remobilized chalcopyrite and in the deformation of pyrite at grain margins. Microscopically, strong shearing of quartz domains (Fig. 3g), which otherwise display a granoblastic fabric (Fig. 3m), is also noted in association with retrogressive formation of chlorite. Embayment between quartz and deformed aggregates of pyrite indicates that their present fabric is the result of shearing (Fig. 3n). Similar relationships can be interpreted for other two- or multi-component assemblages that involve minerals such as quartz, apatite, chalcopyrite, cobaltite and pyrite. The characteristic feature is a caries-type boundary associated with close-to-plastic deformation in the less-refractory mineral present at the contact (e.g., apatite against quartz, or chalcopyrite against cobaltite and apatite, Fig. 3o). This implies that shearing is subsequent to formation of the main sulfide-gangue assemblage in the vein, since tectonic reworking of any of the mutual boundaries involves corrosion of the more refractory minerals assisted by local remobilization of the more ductile ones.

During shearing, both cobaltite and chalcopyrite were remobilized from the larger sulfide masses, forming the oblique trails mentioned above. This is evidenced by lamellae of cobaltite crosscutting pre-existing chalcopyrite-quartz boundaries, and blebs of both minerals that occur at fracture junctions (Fig. 4a). The blebs have morphologies suggestive of plastic deformation, indicating solid-state ductile remobilization from the main sulfide mass. Although cobaltite has a less plastic behavior than chalcopyrite, it shows this type of ductile transport more often. Nucleation of cobaltite, sometimes on pre-existing pyrite nuclei, is also noted, for example in pressure shadows of refractory mineral grains (e.g., feldspar at the contact to chlorite) that were brecciated.

In contrast to cobaltite, chalcopyrite is more often incorporated within bundles of chlorite that crosscut previously formed mineral boundaries. Chlorite lamellae and chalcopyrite are intergrown within these bundles (Fig. 4b), indicating that new chlorite formed from fluids that infiltrated during the shearing event and assisted small-scale solid-state remobilization of chalcopyrite from the nearest larger patch. This event is also marked by formation of thin shears of monazite in deformational

knots (Fig. 4c), as well as nucleation of small grains of allanite-(Ce) noted within pressure shadows at the margins of deformed pyrite. Such textures indicate that the deformation also affected the distribution of REE within the vein.

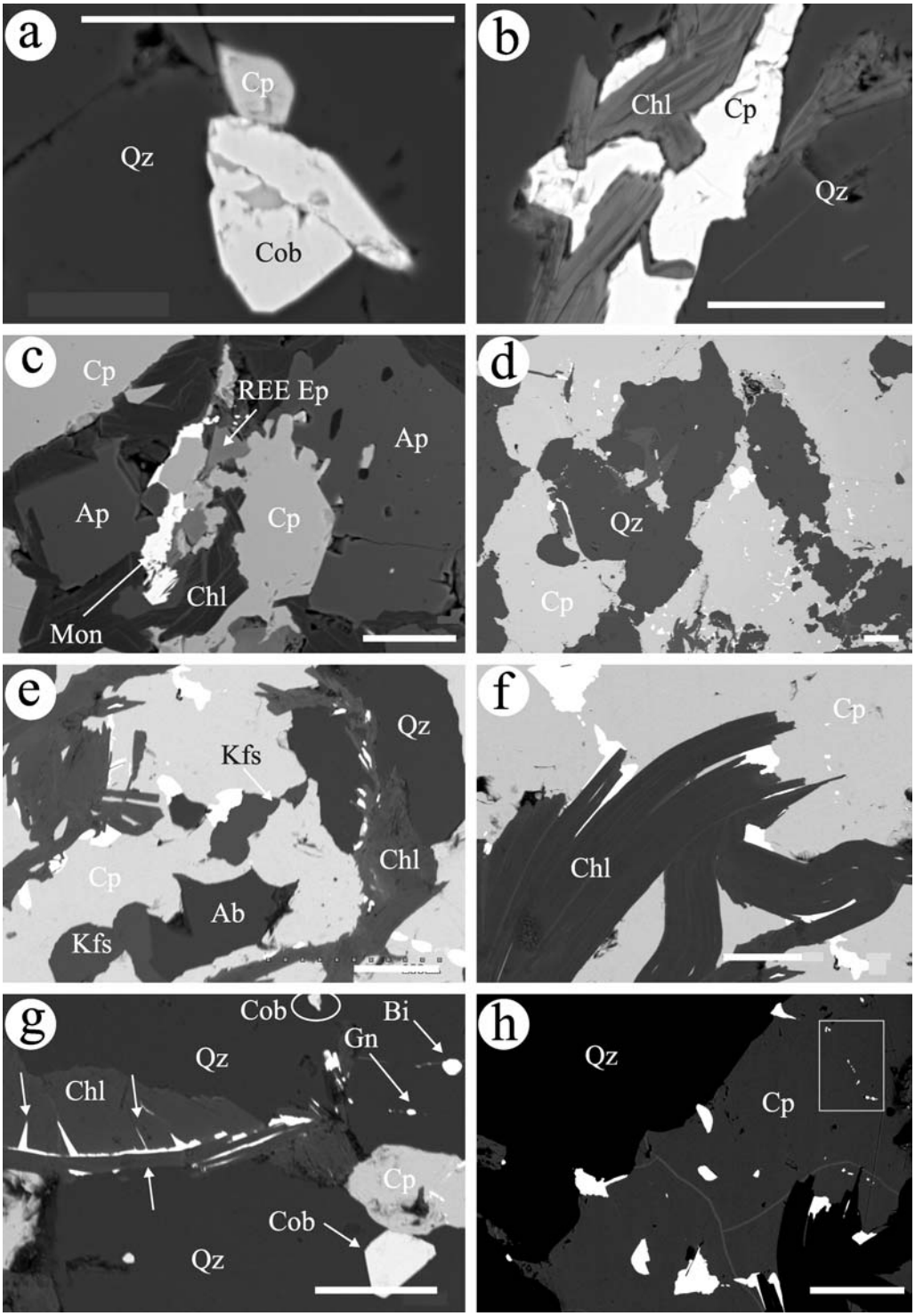

The Au–Bi–Te association

Gold and Bi-minerals occur together as patches and blebs clustered around brecciated and deformed quartz that is enclosed within chalcopyrite (Fig. 4d). Brecciation is present in all minerals surrounding, or at the margins of, chalcopyrite (e.g., epidote, REE-carbonate and cobaltite, Fig. 3a, d, f). It is also in these areas that chlorite is observed in abundance coexisting with feldspar (Fig. 4e).

Assemblage and morphology

The blebs and patches of Bi-minerals occur in chlorite lamellae that crosscut boundaries between chalcopyrite and quartz (Fig. 4e), but they also form trails perpendicular to chlorite, extending into the adjacent chalcopyrite or quartz (Fig. 4f). Such crosscutting trails are observed where the chlorite lamellae are deformed and folded, indicating that the blebs are not found in compressional domains (within the fold). The preference of Bi-minerals for dilational sites is also inferred from the observation that they fill spaces between the chlorite lamellae that have a fan-like arrangement (Fig. 4g). Moreover, they appear with a droplet-shape (native Bi always occurs as droplets) formed in shear gashes along fractures within quartz. Several blebs of galena were also observed along trails parallel to the native Bi. Also in Fig. 4g, this trail perpendicularly crosscuts another fracture containing cobaltite–chalcopyrite blebs. An idiomorphic grain of cobaltite occurs at the other side of the chalcopyrite mass where this fracture stops. This indicates that such fractures are relevant for ore remobilization within the vein and the local topology will control the morphology of the resulting minerals. However, morphology alone does not discriminate between mechanisms that produce remobilization.

Large patches of Bi-minerals occur within chalcopyrite. The average size of the patches is from 10 to several tens of μm, rarely up to several hundred μm; the smallest are down to a few μm. Their morphology varies from rounded to lens-like

Fig. 4. Back-scattered electron images showing aspects of remobilization. **a** Blebs of cobaltite and chalcopyrite formed at fracture junction in quartz. Note ductile deformation of the blebs. **b** Remobilized chalcopyrite within a bundle of chlorite. The two are intertwined along the shear-trails. **c** Edge of chalcopyrite with thin patches of monazite. They are formed in a compression knot realised between blasts of apatite surrounded by chlorite. **d** Field of blebs/patches bearing the Au–Bi–Te association (bright white) within chalcopyrite. They cluster around brecciated quartz and follow some of the chlorite lamellae. **e** Bi-minerals (bright white) along chlorite lamellae that crosscut chalcopyrite-quartz boundaries. Note also the presence of feldspar. **f** Trail of blebs/patches containing the Au–Bi–Te association (bright white) crosscutting folded chlorite lamellae. **g** Aspects of remobilization within quartz enclosed in chalcopyrite: (i) Bi-minerals (white) filling the spaces between 'fan-like' lamellae of chlorite (left of figure), (ii) Droplets of native Bi and galena along shear gashes, (iii) Crosscutting fracture with blebs of cobaltite + chalcopyrite (upper part), (iv) idiomorphic cobaltite formed on the other side of chalcopyrite. **h** Typical trails of blebs/patches containing the Au–Bi–Te association within chalcopyrite. Note the variable morphology of the patches/blebs (see text). The rectangle marks trails following fractures that were wetted by fluids (marked by formation of chlorite and feldspars). Abbreviations as for Fig. 3 and Bi – native bismuth, Gn – galena, Mon –monazite. All scale bars: 50 μm

blebs, to less abundant thin elongate patches. In most cases, a single bleb or patch shows a combination of curved and angular edges (Fig. 4h). There is also a tendency to form amoeboid-like blebs, especially at contacts between chalcopyrite and another mineral. Some of the blebs occur along thin cracks, marked by discrete platelets of chlorite and/or feldspar grains. Even though this is observed only rarely, it is nonetheless clear that the trails follow planes of micro-shearing within chalcopyrite, and the deposition of Bi-minerals along them probably exploits any porosity created or structures developed (e.g., cleavage) during the shearing of the host sulfide.

Mineral assemblages and their textural relationships

The Au–Bi–Te association (Figs. 5–7) consists mainly of Bi-sulfosalts, i.e., oversubstituted bismuthinite (BD_{10}; ideally $Cu_{0.4}Pb_{0.4}Bi_{7.6}S_{12}$) and cosalite (ideally $Pb_2Bi_2S_5$); jonassonite (ideally $AuBi_5S_4$), native Au and several Bi-sulfotellurides and -selenides: ingodite [Bi(Te,S)], ikunolite [$Bi_4(S,Se)_3$] and laitakarite [$Bi_4(Se,S)_3$]. Single-component blebs are observed in abundance only for bismuthinite, seldom for native Au and jonassonite, and very rarely for native Bi. Native gold, when alone, occurs as tiny droplets; nearly always these are situated in the vicinity of blebs of Bi-minerals. Otherwise, most of these minerals exist in two-, three-, and more rarely four-component blebs or patches. Most of the native gold appears either as rounded droplets or more rarely as lamellae within BD_{10}. It also occurs as minute inclusions in assemblages between a sulfosalt and jonassonite. In larger patches, curvilinear boundaries occur between native gold and its host sulfosalt.

Jonassonite, native Au and Bi-(Pb) sulfosalts

Jonassonite, which never exceeds 30 μm in size, is most commonly spatially associated with cosalite (Fig. 5a, b, d, f, g), although it may also occur with BD_{10}

Fig. 5. Back-scattered electron images showing associations and morphology of blebs/patches that include Au-minerals. All are hosted within chalcopyrite. **a** Jonassonite with cosalite at the tip of the patch. Note the combination of rounded and angular edges. **b** Curvilinear boundaries between jonassonite and cosalite. **c** Deformed boundaries between jonassonite and oversubstituted bismuthinite (BD_{10}). **d** Typical association of jonassonite with cosalite. **e** Triple junction between cosalite, jonassonite and native gold. **f** Patch with angular edges controlled by cleavages in chalcopyrite. Note the inter-layering contact between both jonassonite and ingodite and host cosalite; ingodite also as exsolution spots (see Fig. 7i for detail). **g** Patch with similar angular edges, showing association of jonassonite, ikunolite and cosalite. **h** Lamellae of native gold within BD_{10}. Note the amoeboid terminations of the patch. **i** 'Tulip'-shaped bleb containing native gold with cuspate boundaries between cosalite and BD_{10}; this is continuation of a curvilinear limit between the two sulfosalts. Note also the differences in the outline boundary of the two sulfosalts with chalcopyrite; wavy at the margin of softer BD_{10}, and straight along cosalite. **j** Native gold as marginal inclusions in BD_{10}. The upper edge is formed by cosalite with lamellae of ingodite (see Fig. 7h for detail). Abbreviations: Au – native gold, Cos – cosalite, Ing – ingodite, Iku – ikunolite, Jon – jonassonite

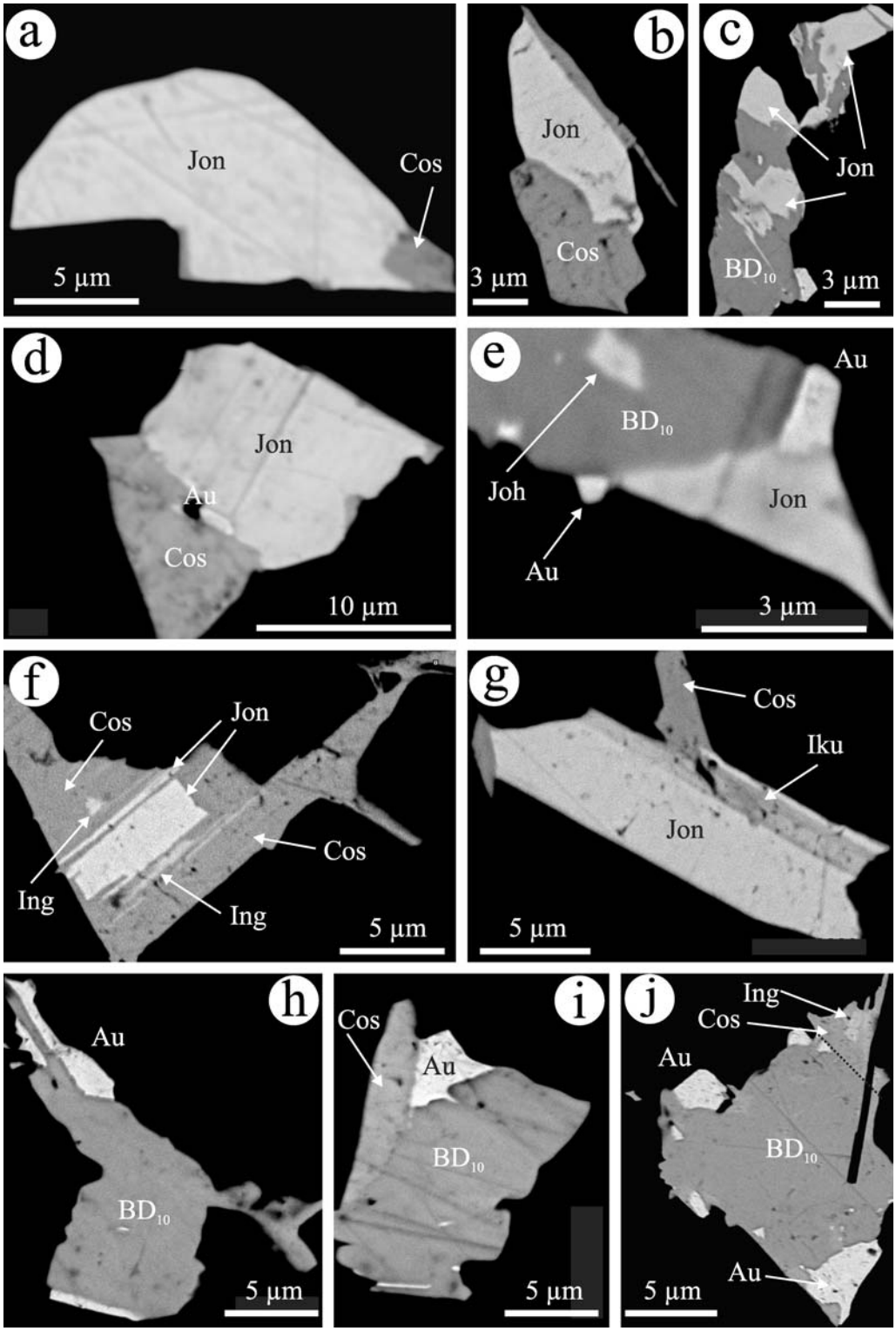
a
Jon
Cos
5 µm
b
Jon
Cos
3 µm
c
Jon
BD10
3 µm
d
Jon
Au
Cos
10 µm
e
Au
BD10
Joh
Jon
Au
3 µm
f
Cos
Jon
Cos
Ing
Ing
5 µm
g
Cos
Iku
Jon
5 µm
h
Au
BD10
5 µm
i
Cos
Au
BD10
5 µm
j
Ing
Cos
Au
BD10
Au
5 µm

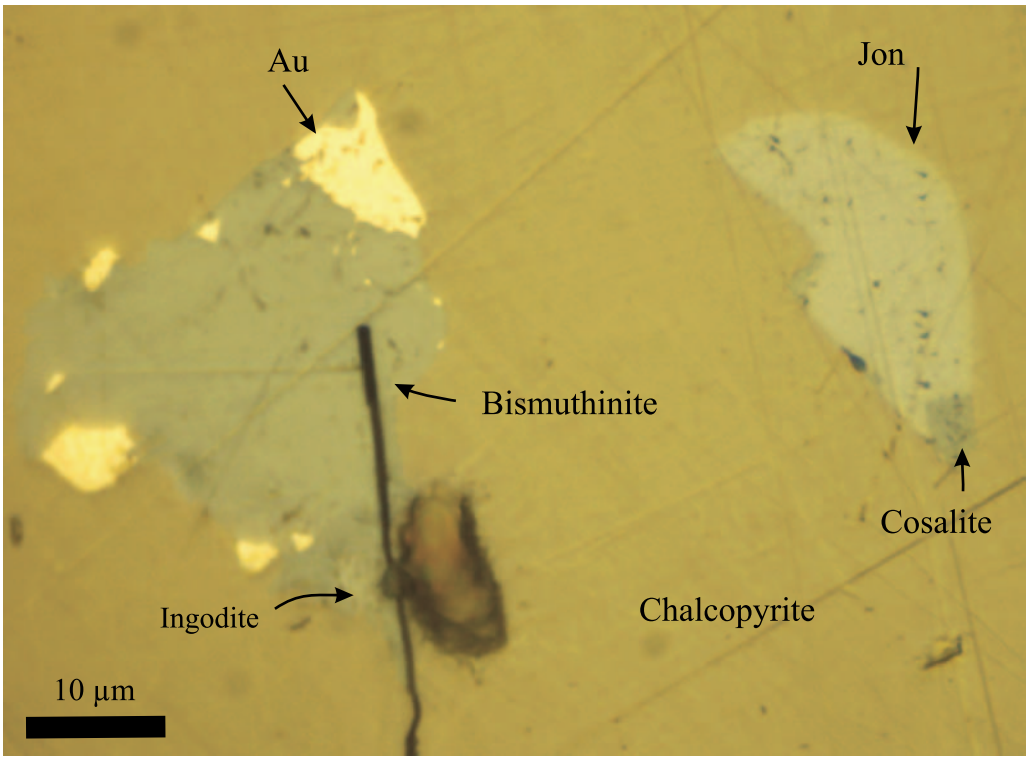

Fig. 6. Reflected light microphotograph, in oil immersion, showing the optical characteristics of jonassonite (same patch as in Fig. 5a; see also text). The patch (to the left) with native gold and BD_{10} (shown also in Fig. 5j) is included for comparison

(Fig. 5c, e). In contrast to native gold, jonassonite tends to occupy at least half of the respective bleb, instead of being dispersed throughout it, or towards the edges, as small inclusions. Under the microscope, jonassonite is white-bluish in color when immersed in oil, comparable with ingodite, although slightly more yellow in color (Fig. 6). The reflectivity of jonassonite is comparable with ingodite, and

Fig. 7. Back-scattered electron images of Bi–(Pb)–sulfosalts and sulfotellurides/selenides (**a**–**g**); textural details (h and i) for selected areas in some of the patches in Fig. 5. **a** Assemblage with cosalite and BD_{10}. Branched strips of ingodite are exsolved from BD_{10} and are shown in detail in Fig. **b**. **c**, **d** Cuspate lamellae (**c**) and dusty inclusions (**d**) of ingodite contained within BD_{10}. **e** Square-shaped inclusions of laitakarite in BD_{10} formed at the contact with a cosalite lamella. **f** Triple-junction with curvilinear boundaries between cosalite, BD_{10} and ingodite. The low-angle contact between ingodite and cosalite displays thin inter-layering banding shown in detail in **g**. **h** Detail of patch in Fig. 5j showing a similar texture between ingodite and host cosalite. Also note that the native gold blebs are enclosed only within BD_{10}. **i** Detail of the same type of contact between jonassonite and cosalite within the patch from Fig. 5f. Note the splitting of the jonassonite band towards the edge and also the interfingering contact at the upper part of the main area with jonassonite (arrowed). See also the strips and spots of ingodite. Abbreviations as in Fig. 5 and Ltk – laitakarite

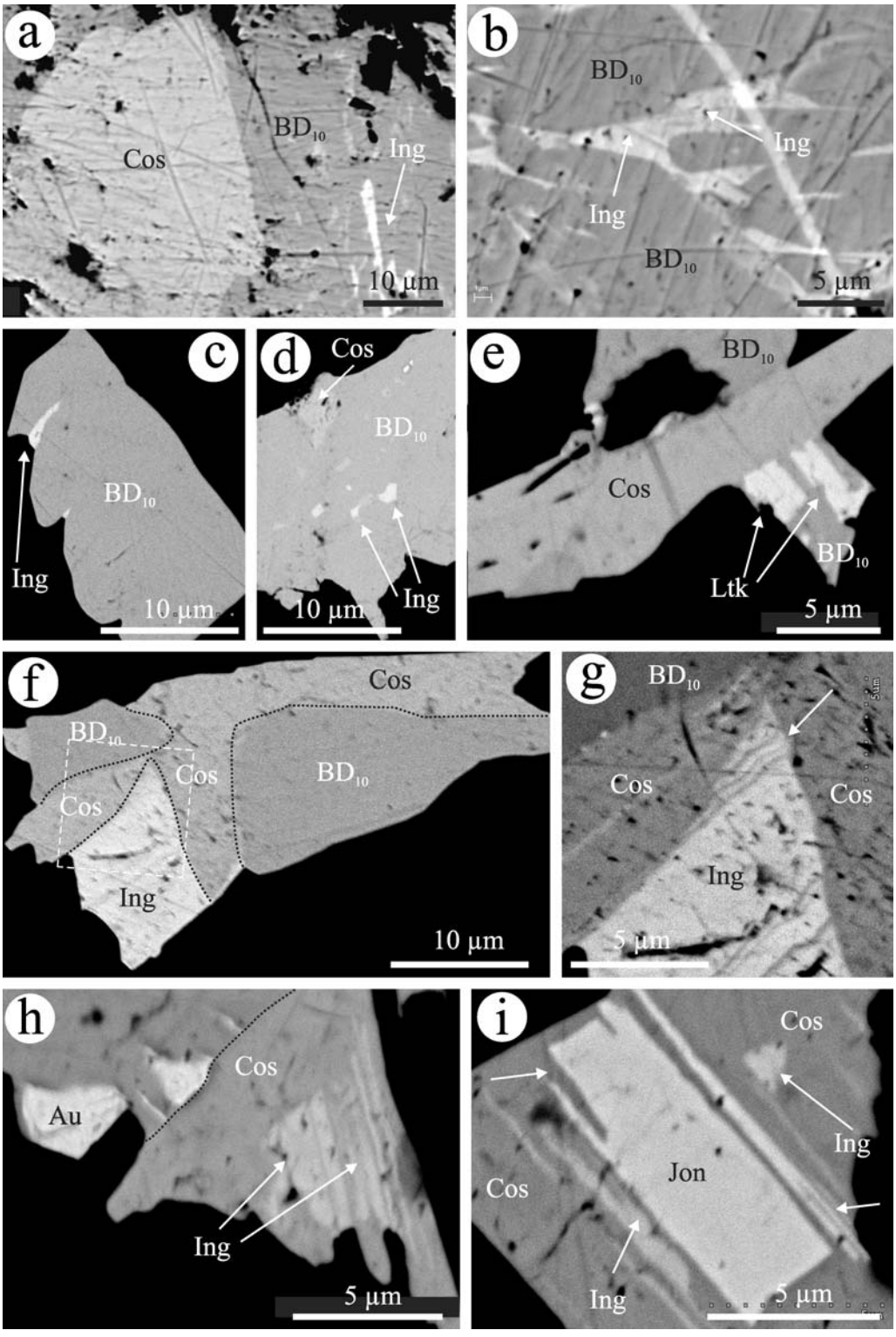
a
Cos
BD10
Ing
10 µm
b
BD10
Ing
Ing
BD10
5 µm
c
BD10
Ing
10 µm
d
Cos
BD10
10 µm
Ing
e
BD10
Cos
Ltk
BD10
5 µm
f
Cos
BD10
BD10
Cos
Cos
Ing
10 µm
g
BD10
Cos
Cos
Ing
5 µm
h
Cos
Au
Ing
5 µm
i
Cos
Ing
Jon
Cos
Ing
5 µm

notably higher than cosalite. Jonassonite has a weak anisotropy under crossed polars. The mineral takes a better polish than cosalite and has a slightly higher polishing hardness. Mutual boundaries between jonassonite and the accompanying sulfosalt may be curvilinear (Fig. 5a, b). We point to the wide variation in the morphology of the blebs dominated by jonassonite (Fig. 5a–g), which indicate control by local porosity in conjunction with the presence of cleavage planes in the host chalcopyrite (as seen in the combination of both rounded and straight edges, Fig. 5a). Patches such as those in Fig. 5e and g, seem to be controlled mostly by cleavage planes in chalcopyrite.

More rarely, mutual boundaries between jonassonite and the host sulfosalt appear deformed (Fig. 5c), indicating readjustment during or post crystallization within the blebs. Otherwise these boundaries are straight (Fig. 5d–g), with jonassonite showing a tendency towards idiomorphic development against the associated sulfosalts or telluride. Triple-point junctions are also noted between jonassonite, BD_{10} and native gold (Fig. 5e), indicating crystallization at equilibrium. Most interesting, however, is the interlayering between jonassonite and host cosalite (Fig. 5f). Emphasizing the apparent layering between the phases within this patch are thin strips of ingodite on the other side of the main body of jonassonite (Fig. 5f); the telluride also forms a scatter of exsolved spots inside the cosalite.

The BD_{10} blebs hosting native gold have amoeboid terminations (Fig. 5h) or tulip-like morphologies (Fig. 5i). In the patches containing BD_{10} and cosalite (ingodite may also be present), native gold preferentially occurs within BD_{10} (Fig. 5j). Cuspate (low angle) boundaries between native gold and the two sulfosalts in Fig. 5i are characteristic, as are also the curvilinear boundaries (Fig. 5j).

Bismuth sulfotellurides/selenides

Bismuth sulfotellurides/selenides occur only as inclusions within sulfosalts. Ingodite is by far the most common sulfotelluride and may be present in either of the two sulphosalts, i.e., BD_{10} and cosalite. In BD_{10}, ingodite occurs as exsolutions with various morphologies, i.e., as thin branched strips (Fig. 7a, b), cuspate lamellae (Fig. 7c) and dusty inclusions (Fig. 7d). Laitakarite was rarely observed as inclusions in the same sulfosalt (Fig. 7e).

Triple junctions with curvilinear boundaries were noted between ingodite and the two sulfosalts (Fig. 7f). In detail, at the low-angle corner between ingodite and cosalite, the boundary is split into a series of thin narrow bands that dissipate into the cosalite (Fig. 7g). Alternating repetitive banding between ingodite and cosalite is observed in one of the 4-component patches (Fig. 7h). The other two components are BD_{10} and native gold; the latter appears as exsolved blebs within BD_{10} but not in cosalite. The contact between ingodite and cosalite strongly resembles the one between jonassonite and cosalite (Fig. 7i).

Microanalytical data for ore minerals

Electron probe microanalytical data were collected using a Cameca SX-51 instrument at Adelaide Microscopy Centre, University of Adelaide, Australia. Operating conditions were 20 kV accelerating voltage and 19.5 nA beam current. Standards

Table 1. *Electron microprobe analyses of jonassonite, ikunolite, laitakarite, ingodite and sulphosalts*

Jonassonite		Analysis (wt.%)									Total	Calculated formula (on the basis of 10 atoms p.f.u.)
		Cu	Ag	Au	Pb	Bi	Sb	S	Se	Te		
mean ($n=9$)		–	0.04	14.43	6.48	69.07	<mdl	9.06	<mdl	<mdl	99.08	$Au_{1.02}(Bi_{4.60}Pb_{0.43})_{5.04}S_{3.94}$
Std. Dev.		–	0.04	0.22	0.79	0.49		0.33	<mdl	<mdl		
Minimum		–	<mdl	14.15	5.57	68.34	<mdl	8.75	<mdl	<mdl		
Maximum		–	0.12	14.82	7.49	70.02	<mdl	9.69	<mdl	<mdl		
representative analyses	Fig. 5a	–	0.02	14.48	5.93	69.33	<mdl	8.80	<mdl	<mdl	98.56	$Au_{1.04}(Bi_{4.68}Pb_{0.40})_{5.09}S_{3.87}$
	Fig. 5b	–	0.07	14.63	7.22	69.34	<mdl	9.69	<mdl	<mdl	100.94	$(Au_{1.00}Ag_{0.01})_{1.01}(Bi_{4.46}Pb_{0.47})_{4.93}S_{4.06}$
	Fig. 5f	–	<mdl	14.28	6.94	69.16	<mdl	9.23	<mdl	<mdl	99.61	$Au_{1.00}(Bi_{4.57}Pb_{0.46})_{5.03}S_{3.97}$
	Fig. 5d	–	0.04	14.22	7.49	69.22	<mdl	9.29	<mdl	<mdl	100.25	$(Au_{0.99}Ag_{0.01})_{1.00}(Bi_{4.54}Pb_{0.50})_{5.03}S_{3.97}$
	Fig. 5d	–	<mdl	14.15	7.47	68.62	<mdl	9.31	<mdl	<mdl	99.54	$Au_{0.99}(Bi_{4.52}Pb_{0.50})_{5.02}S_{4.00}$
Ikunolite representative analysis*		–	<mdl	–	17.20	71.25	<mdl	9.73	1.40	0.53	100.10	(on the basis of 7 atoms p.f.u.) $(Bi_{3.19}Pb_{0.78})_{3.96}(S_{2.83}Se_{0.17}Te_{0.04})_{3.04}$
Laitakarite representative analysis*		–	<mdl	–	6.34	77.61	<mdl	4.46	12.70	0.88	101.99	$(Bi_{3.67}Pb_{0.30})_{3.97}(Se_{1.59}S_{1.37}Te_{0.07})_{3.03}$
Ingodite mean* ($n=8$)		–	<mdl	–	2.39	73.17	<mdl	6.26	3.45	16.64	101.91	(on the basis of 2 atoms p.f.u.) $(Bi_{0.96}Pb_{0.03})_{0.99}(S_{0.53}Te_{0.36}Se_{0.12})_{1.01}$
Bismuthinite (BD_{0-10})												(on the basis of 5 atoms p.f.u.)
mean ($n=5$)		0.69	<mdl	–	1.48	78.06	0.07	18.20	0.03	0.03	98.56	$(Bi_{1.95}Pb_{0.04}Cu_{0.06})_{2.04}S_{2.96}$
mean* ($n=9$)		1.18	0.04	–	5.48	76.70	0.07	18.65	0.39	<mdl	102.51	$(Bi_{1.84}Pb_{0.13}Cu_{0.09})_{2.07}(S_{2.91}Se_{0.03})_{2.93}$
Cosalite												(on the basis of 9 atoms p.f.u.)
mean ($n=4$)	Fig. 7f	1.13	0.49	–	34.86	46.37	0.03	15.18	2.23	0.36	100.66	$(Bi_{2.18}Pb_{1.65}Ag_{0.04}Cu_{0.17})_{4.05}(S_{4.65}Se_{0.28}Te_{0.03})_{4.95}$
mean ($n=2$)	Fig. 7a	0.12	0.06	–	39.31	42.10	0.12	15.35	0.11	0.06	97.23	$(Bi_{2.07}Pb_{1.95}Ag_{0.01}Cu_{0.02}Sb_{0.01})_{4.06}(S_{4.92}Se_{0.01}Te_{0.01})_{4.94}$

– Not analysed

* SEM-EDS analysis (electron microprobe analysis gave poor totals)

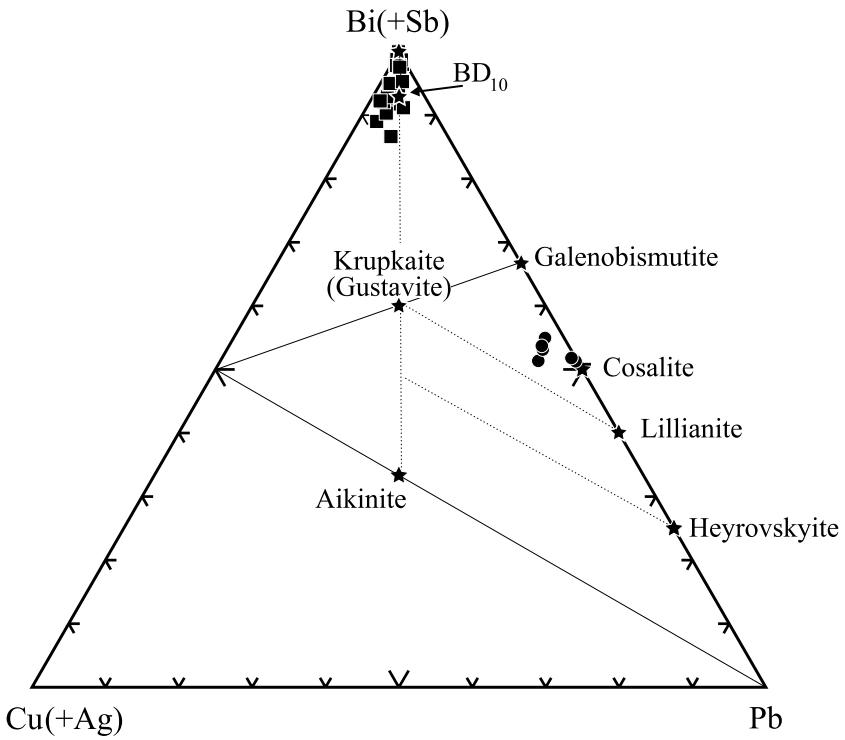

Fig. 8. Compositional data for Bi–(Pb) sulfosalt minerals, expressed in terms of Bi(+Sb)–Cu(+Ag)–Pb. Full circles – cosalite; squares – BD_{10}

used were: Bi_2Se_3 (Bi), PbS (Pb, S), Ag (Ag), Cu (Cu), Sb_2S_3 (Sb), Te (Te). These data are supplemented by data collected using a Hitachi scanning electron microscope equipped with an Oxford Instruments wavelength-dispersive spectrometer at the Natural History Museum, University of Oslo.

Compositional data for the two sulfosalts in the above assemblages (Table 1) are plotted in the (Ag + Cu)–Bi–Pb ternary diagram (Fig. 8). The cluster of points representing oversubstituted bismuthinite range from close to BD_0 to BD_{10}, with a marked tendency towards Cu–Pb-rich compositions in blebs that contain Au-minerals. Cosalite in larger patches (e.g., Fig. 7a) plots close to ideal $Pb_2Bi_2S_5$, whereas cosalite in association with Au-minerals contains more significant amounts of Ag and Cu.

Compositional data for the sulfotellurides and sulfoselenides are shown in Table 1 and plotted in Fig. 9. Both laitakarite $\sim Bi_4(Se,S)_3$ and ikunolite $Bi_4(S,Se)_3$ exhibit values of $S/(S + Se) = 0.34$–0.45 for laitakarite and 0.92–0.94 (plus one outlier at 0.64) for ikunolite. Both minerals carry significant amounts of Pb (exceeding 0.71 and 1.20 a.p.f.u., respectively), as well as minor Te. Ingodite, the most abundant sulfotelluride, displays a limited spread of compositions, with the $(Te + Se)/(Te + S + Se)$ ratio varying from 0.42 to 0.54 and $(Bi + Pb)/(Te + S + Se)$ ranging from 0.9 to 1.06. Some analyses of the smallest (sub-5 μm) telluride grains, generally those closely associated with ingodite show exceptionally high contents of Pb, suggesting that fine intergrowths of various Bi–Pb–Te–S minerals (aleksite group; *Cook* et al., in press) may be present in the assemblage.

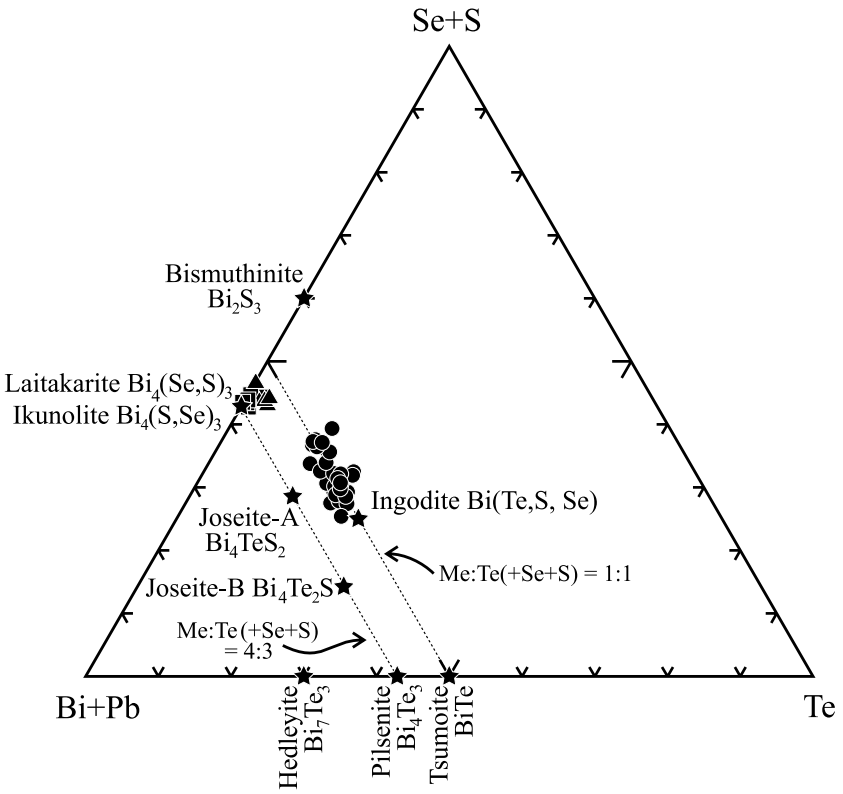

Fig. 9. Compositional data for sulfotellurides and sulfoselenides, expressed in terms of (Bi + Pb)–(Se + S)–Te. Full circles – ingodite; triangles – laitakarite; squares – ikunolite

The mean composition of ten grains of jonassonite (Table 1) is: 14.43 wt.% Au, 0.04 wt.% Ag, 69.07 wt.% Bi, 6.48 wt.% Pb, 9.06 wt.% S), giving the empirical formula $Au_{1.02}(Bi_{4.60}\ Pb_{0.43})_{5.04}S_{3.94}$. There is little variation in the data and when plotted, the dataset closely overlaps the field of published data for other occurrences of the phase (Fig. 10a). The Highiş occurrence differs in that the Pb content is somewhat higher than in the other occurrences, ranging from 0.25 to 0.63 a.p.f.u., and it shows a reasonable correlation with Bi content (Fig. 10b). Significant substitution of Pb in jonassonite has until now been known only from occurrences in Hungary (*Dobosi* and *Nagy*, 1989) and Morocco (*Oudin* et al., 1988).

Native gold has a limited compositional field, typically in the range ($Au_{82-84}Ag_{16-18}$). Cobaltite compositions are mostly in the range $Co/(Co + Fe + Ni) = 0.67–0.83$ and $Fe/(Co + Fe + Ni) = 0.16–0.29$, with $\Sigma(Co + Fe + Ni) \sim 1$, $\Sigma(As + Sb) \sim 0.95$ and $S \sim 1.05$. The zoning patterns are expressed in terms of varying $Co/(Co + Fe + Ni)$ (Fig. 3a).

Jonassonite

Jonassonite was first reported as a single grain, 15 by 40 μm in size, with composition $Au_{1.06}Bi_{4.93}S_{4.01}$, from a Au–Bi–W–tourmaline-quartz vein related to a Miocene granite stock, Tsugahira Mine, southern Kyushu, SW Japan (*Hamasaki* et al.,

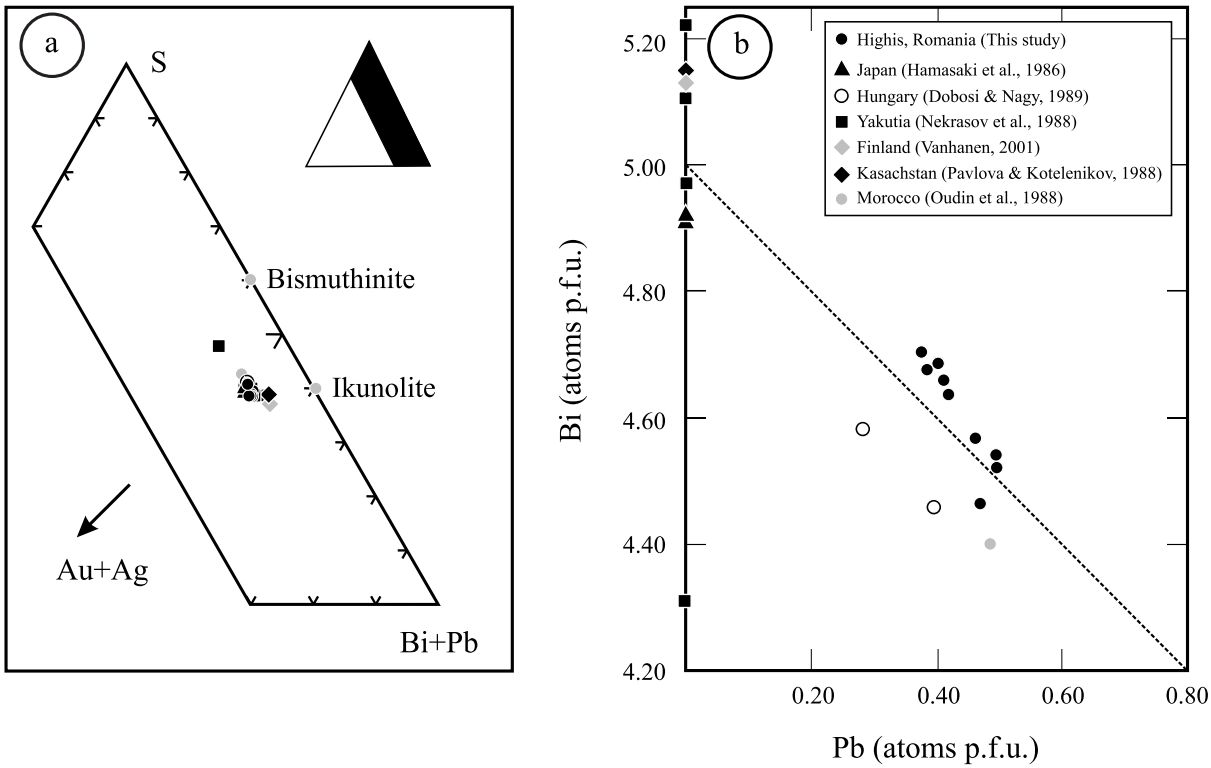

Fig. 10. Compositional data for jonassonite from the occurrence in the Highiş Massif, and comparison with published data from other occurrences. **a** Ternary diagram in (Bi + Pb)–(Au + Ag)–S space. **b** Correlation of Bi and Pb contents on 10-atom formula unit basis

1986). It has since been described from a number of additional localities including occurrences in northeastern Yakutia (*Nekrasov* et al., 1988), Nagybörzsöny, Börzsöny Mts., northern Hungary (*Dobosi* and *Nagy*, 1989), Kazakhstan (*Pavlova* and *Kotelinikov*, 1988), the Tichka Massif, High Atlas, Morocco (*Oudin* et al., 1988) and the Paleoproterozoic Kuusamo Schist Belt, northeast Finland (*Vanhanen*, 2001). In each of these occurrences, jonassonite is part of a pronounced Bi-association: either Bi-sulfosalts (Nagybörzsöny), Bi-tellurides (Yakutia), or both sulfosalts and tellurides (as in the Highiş occurrence). Although the phase is generally only present as a trace constituent, it can also form mineable concentrations, for example in the New Occidental deposit, Cobar District, NSW, Australia (called '*newoccidentallite*' by *Stegman*, 2001). We note that in these occurrences, both native bismuth and native gold are present. Maldonite is present only in some of the above occurrences, and has not been identified in the Highiş occurrence. Compositional data show limited deviation of the Pb/(Bi + Pb) ratio from ideal stoichiometry. At Highiş, the mineral contains up to 9.56 wt.% Pb. *Dobosi* and *Nagy* (1989) reported 5.95 wt.% Pb in unnamed $AuBi_5S_4$ from Nagybörzsöny; *Oudin* et al. (1988) reported 4.76 at.% Pb in the phase from the Tichka occurrence. The published descriptions differ: *Hamasaki* et al. (1986) considering the phase, like us, as light grayish white in color and distinctly anisotropic, ''like joseite-B'', whereas *Nekrasov* et al. (1988) considered the phase as grey and isotropic. Full

characterization of $AuBi_5S_4$, and naming of the compound as jonassonite, was only recently made (*Paar* et al., 2006).

Discussion

Ore genesis

The most prominent feature of the assemblages in the Şoimuş Ilii vein is the retrograde metamorphic overprinting recorded during the shearing event(s) (Fig. 3). This is important because it was previously unrecognized and also because it is critical to our discussion on the formation of the gold mineralization.

Primary and inherited features

Despite the overprinting, primary textures are not completely obliterated, as locally preserved granoblastic texture involving quartz are indicative of hydrothermal deposition. The marked REE-rich signature of the vein is perhaps the best evidence for a link to a granite-related genesis, as suggested by *Ianovici* et al. (1976). The presence of exsolved pentlandite in pyrrhotite is, however, indicative of an inherited basalt-type mineralization, supporting, at least partially, the earlier view that the ore also has a basic affiliation (*Giuşcă*, 1957; *Brana*, 1958). Despite this, there is no unambiguous evidence to suggest that the Cu ore was entirely formed from hydrothermal fluids associated with a supposed basic intrusion at depth. We propose an interaction between granite-derived fluids and basaltic hornfels and note the indirect evidence for incorporation of fragments of these rocks within the vein (e.g., $Mg/(Mg + Fe)$ zonation trends in chlorite inferring formation after actinolite in the hornfels). The vein is also characterized by the conspicuous abundance of primary apatite, as well as a Co–Bi-rich trace mineral signature (cobaltite, native Bi and Bi-sulfosalts; *Giuşcă*, 1957; this study).

Overprinting and remobilization

Infiltration of fluids during shearing (metamorphogenic hydrothermal fluids) is evident not only from retrogression of a pre-existing hornfels assemblage that involves biotite, amphibole and feldspar, but also from formation of new feldspars and chlorite along foliation planes, as well as the brecciation that crosscuts former mutual boundaries between chalcopyrite and quartz.

Based upon the presence of adularia, we estimate a neutral to weakly-reducing character for the metamorphogenic fluids. The chlorite-albite-epidote association indicates that metamorphism associated with the shearing episode was at the greenschist facies. The coexistence of biotite and chlorite indicates metamorphic conditions towards the upper greenschist facies. Peak temperatures of ca. 400 °C are suggested by the prevailing assemblages and are consistent with estimations given by *Pană* and *Erdmer* (1994) for Alpine greenschist shear zones in the Apuseni Mountains and Romanian Carpathians.

On the basis of textural data, we have shown that the shearing also assisted redistribution of REE within the vein and caused local remobilization of sulfides

(e.g., chalcopyrite, cobaltite, and most importantly the Bi-minerals, Fig. 4). In contrast to the two sulfides, which are mostly remobilized in shears and folds, the Bi-minerals occur within dilational sites formed during shearing and fluid circulation (e.g., shear gashes, filling fan-like spaces between chlorite lamellae, or within pores and along cleavages in chalcopyrite). Textural evidence (e.g., bleb/patch morphology, curvilinear and cuspate low-angle mutual boundaries within the blebs, Figs. 5–7), are in favor of the formation of Bi-minerals as the result of crystallization from melt precipitates. We will hence discuss formation of the association Au–Bi–Pb–(Cu)–S–Te–(Se) within the hypothesis that the minerals formed are the products of remobilization, and were transported as melts during shearing.

Neither chalcopyrite nor cobaltite are seen within the Bi-mineral blebs, inferring that they did not melt but instead underwent small-scale remobilization in the solid-state, as would be expected from their ductile behavior during deformation at temperatures below 400 °C (e.g., *Marshall* and *Gilligan*, 1993). The same applies to galena, a sulfide with high-melting point (1118 °C; e.g., *Craig*, 1967), which is occasionally observed remobilized within shear gashes (Fig. 4g).

The size of the Bi-mineral patches described here are three orders of magnitude smaller than the ones reported by *Giuşcă* (1957). Secondly, the Bi-mineral association differs from the one at the margin of the vein in that Bi-sulfosalts are the main components rather than native bismuth. Thirdly, the galena that forms swarms of skeletal and rounded inclusions within native Bi (*Giuşcă*, 1957) is not present in the Bi-mineral patches described here. We thus consider that the Bi-mineral association (i.e., native Bi and Bi-sulfosalts, at the margin of the vein may have been a source for the melts that incorporated and concentrated Au during remobilization). The source of Au may either be in the vein assemblage or in the primary Bi-mineral association itself, presumably at very low concentrations in either case.

Melt involvement in formation of the Au–Bi–Te association

Native gold and jonassonite occur in close paragenetic association with Bi–(Pb)-sulfosalts and -tellurides in the Şoimuş Ilii vein (Figs. 5 and 6). The presence of elements of the LMCE group (*Frost* et al., 2002), such as Bi, Pb, and Te, raises the question of partial melting of a pre-existing ore and consequent precious metal remobilization during the metamorphic event that overprinted the hornfels-hosted ore. *Tomkins* and *Mavrogenes* (2002) and *Tomkins* et al. (2004) documented the involvement of LMCE-derived melts in Au remobilization for deposits that experienced high-grade metamorphism at temperatures in excess of 600 °C. We will discuss this type of model for the shear-remobilizates in the vein in the Highiş Massif, where metamorphism is at upper greenschist facies, with temperatures probably not greatly exceeding 400 °C.

The compositions of individual blebs in the Au–Bi–Pb–Te–S association reflects assemblages from bi-component (Bi–S), tri-component (Au–Bi–S, Bi–S–Te), and four-component systems (Au–Bi–Pb–S, Au–Bi–S–Te, Bi–Pb–S–Te) (Table 2), if we ignore the minority of blebs with co-existing Se-bearing minerals. In each of the above systems, we note the presence of both Bi and S. Considering the presence of Pb, not only in cosalite, a Bi–Pb sulfosalt, but also in oversubstituted bismuthinite (BD_{10}), Bi-tellurides and jonassonite, Pb is omnipresent, even if

Table 2. *Types of assemblages found in the Au–Bi–Pb–S–Te–(Se) association*

Figure	Melt composition calculated from mineral components at 1:1 ratio (a.p.f.u.)	Gold minerals		Bi–sulphosalts		Bi–tellurides(selenides)	
		Gold	Jonassonite	BD_{10}	Cosalite	Ingodite	Ikunolite/ laitakarite
5h	$(AuBi_2)_3S_3$	Au		$Cu_{0.4}Pb_{0.4}Bi_{7.6}S_{12}$			
5i	$(AuBi_4Pb_2)_7S_8$	Au		$Cu_{0.4}Pb_{0.4}Bi_{7.6}S_{12}$	$Bi_2Pb_2S_5$		
5j	$(AuBi_5Pb_2)_8(S,Te)_9$	Au		$Cu_{0.4}Pb_{0.4}Bi_{7.6}S_{12}$	$Bi_2Pb_2S_5$	Bi(Te,S)	
5e	$(Au_2Bi_7)_9S_7$	Au	$AuBi_5S_4$	$Cu_{0.4}Pb_{0.4}Bi_{7.6}S_{12}$			
5d	$(Au_2Pb_2Bi_7)_{11}S_9$	Au	$AuBi_5S_4$		$Bi_2Pb_2S_5$		
5a, b	$(AuPb_2Bi_7)_{10}S_9$		$AuBi_5S_4$		$Bi_2Pb_2S_5$		
5f	$(AuBi_8Pb_2)_{11}(S,Te)_{10}$		$AuBi_5S_4$		$Bi_2Pb_2S_5$	Bi(Te,S)	
5g	$(AuBi_{11})_{12}(S,Se)_{12}$		$AuBi_5S_4$		$Bi_2Pb_2S_5$		$Bi_4(S,Se)_3$
5c	$(AuBi_7)_8S_7$		$AuBi_5S_4$	$Cu_{0.4}Pb_{0.4}Bi_{7.6}S_{12}$			
7e	$(Bi_8Pb_2)_{10}(S,Se)_{11}$			$Cu_{0.4}Pb_{0.4}Bi_{7.6}S_{12}$	$Bi_2Pb_2S_5$		$Bi_4(S,Se)_3$
7c	$Bi_3(S,Te)_4$			$Cu_{0.4}Pb_{0.4}Bi_{7.6}S_{12}$		Bi(Te,S)	
7d	$(Bi_5Pb_2)_7(S,Te)_9$			$Cu_{0.4}Pb_{0.4}Bi_{7.6}S_{12}$	$Bi_2Pb_2S_5$	Bi(Te,S)	
7a	$Bi_3(S,Te)_4$			$Cu_{0.4}Pb_{0.4}Bi_{7.6}S_{12}$		Bi(Te,S)	
7f	$(Bi_5Pb_2)_7(S,Te)_9$			$Cu_{0.4}Pb_{0.4}Bi_{7.6}S_{12}$	$Bi_2Pb_2S_5$	Bi(Te,S)	

only a minor component of some of the above minerals. Accordingly, we argue that relationships in the Bi–(Pb)–S system are pivotal to modeling of the observed assemblages. The other systems include Au or Te (or both). We also observe that in 10 of the 14 types of assemblage, BD_{10} is present. Minor amounts of Cu need also to be considered, since this is incorporated in BD_{10} (0.4–2.56 wt.% Cu), as well as in cosalite (0.1–2.79 wt.% Cu). In the discussion below, we will, for the sake of simplicity, ignore Cu, as well as Se. Despite this, the prevalence of BD_{10} instead of bismuthinite (BD_0) in the patches and also the presence of Cu within cosalite, are important observations in interpreting the formation of Au–Bi–Pb–Te–S associations (see below).

The Bi–Pb–S system

In the Bi–Pb–S system, there are ca. 15 phases which have been obtained by synthetic experiment; their number, composition and correspondence to minerals in natural specimens varies from author to author (see discussions in *Craig*, 1967; *Hoda* and *Chang*, 1975). Debate exists even around the stabilities of the most common sulfosalts, some of which are present in the Şoimuş Ilii vein. For example, *Hoda* and *Chang* (1975) could not stabilize galenobismutite ($PbBi_2S_4$) below 400 °C, despite the fact that the mineral had been obtained in previous experimental studies (e.g., *Craig*, 1967; *Salanci* and *Moh*, 1969). Later experiments, however, using longer run times established that the upper stability of galenobismutite is as low as 375–390 °C (*Chang* and *Hoda*, 1977). These results are, however, not acknowledged in subsequent reviews of experimental data for the Bi_2S_3–PbS section of the system Bi–Pb–S (*Villars* et al., 1995), where the minimum temperature for melting of any of the Bi–(Pb)-sulfosalts is given as 590 °C (e.g., *Sadykhova*

et al., 1977 in *Villars* et al., 1995). A second example of a phase in this section that has an upper stability temperature below 590 °C is cosalite (425 ± 25 °C; *Craig*, 1967). The latter author failed, however, to obtain synthetic cosalite and the stability limit is constrained only from experiments involving heating specimens of natural cosalite. *Craig* (1967) invoked the presence of impurities (e.g., Cu, Ag, etc.) in natural cosalite (as also in the Highiş material; Table 1), as critical for stabilizing the sulfosalt.

The apparent discrepancy between data obtained from synthetic phases and natural specimens can also be discussed in the context of crystal-structural modularity, which is characteristic for Bi–Pb sulfosalts (e.g., *Makovicky*, 1989). On the other hand, stacking and/or polysomatic disorder at the lattice scale may account for extensive compositional fields in natural specimens (e.g., *Pring* et al., 1999; *Pring* and *Etschman*, 2002). This has implications, in that experiments involving synthetic material may not necessary replicate natural systems given the difficulty to experimentally reproduce cooling paths encountered in geological environments.

The Bi_2S_3–$CuPbBiS_3$ series

The role of minor elements in controlling the stability of a given phase is also seen in the bismuthinite (Bi_2S_3)-aikinite ($CuPbBiS_3$) series (also known as bismuthinite derivatives). This series includes intermediate members obtained from bismuthinite by the coupled substitution: $Pb^{2+} + Cu^{1+} \rightarrow Bi^{3+}$ up to aikinite ($CuPbBiS_3$). Natural specimens show that the individual members represent 2-, 3-, 4- and 5-fold supercells derived from the parent bismuthinite structure. In contrast, experiments involving synthetic specimens of the bismuthinite-aikinite series at 300 °C indicated a complete solid-solution series (no supercell could be obtained; e.g., *Springer*, 1971). Investigation of the system PbS–Cu_2S–Bi_2S_3 at temperatures >300 °C has shown that the solid-solution field of this series persists and slightly expands from 400 to 500 °C (*Chang* and *Hoda*, 1977). High-resolution transmitted electron microscopy studies coupled with annealing experiments (at 225–175 °C) on synthetic material show ordering of Cu and Pb atoms into supercells as a progressive process which is dependant upon the cooling rate (*Pring*, 1995). *Pring* (1995) concluded that many of the extensive compositional fields for each intermediate member reported in natural specimens may represent stacking disorder at the lattice scale rather than solid solution as predicted from synthetic experiments. A limited range of solid-solution is nonetheless accepted for each member of the series, including BD_{10} (*Topa* et al., 2002). This phase, incorporating only a few wt.% Cu and Pb (Table 1), will have an upper stability limit of 300 °C, as established for the entire bismuthinite derivative series (*Springer*, 1971). This is much lower than the melt temperature of 775 °C given for pure bismuthinite (e.g., *Lin* et al., 1990 in *Villars* et al., 1995). The implication is that formation of melts with composition in the BD_{10} range rather than bismuthinite is possible at temperatures of ca. 400 °C, which were reached during the shearing event. Commensurate with data presented above for cosalite at the same temperature, it is reasonable to consider formation of melts with compositions averaging BD_{10} + cosalite, even though such melts are not indicated on phase diagrams for the Bi–Pb–S system

constructed using data from experiments involving synthetic materials (*Villars* et al., 1995).

Melt formation: the role of native Bi and Bi-sulfosalts

Although *Giuşcă*'s (1962) study was based upon optical microscopy only, and may thus carry uncertainty as to the identity of the observed Bi-sulfosalt(s) (cosalite or one of the bismuthinite derivatives instead of galenobismutite), the photographs shown in his study are conclusive for correct identification of native Bi (e.g., polysynthetic twinning). Native bismuth will melt at temperatures as low as 271 °C.

Molten bismuth (Bi_{melt}) is able to incorporate as much as 37 at.% Au (*Okamoto* and *Massalski*, 1983), 18 at.% Te (*Okamoto* and *Tanner*, 1990) and only 5 at.% S (*Lin* et al., 1990 in *Villars* et al., 1995), according to the respective binary phase diagrams for Bi–Au, Bi–Te and Bi–S systems at 400 °C. Thus, if S is ignored, we can hypothetically consider formation of a Bi–Au–Te melt derived from native Bi alone. This is shown on the ternary Bi–Au–Te diagram at 402 °C, as a melt domain in the Bi apex which is much larger than the one close to the Te apex (*Gather* and *Blachnik*, 1974). Upon cooling, this melt will record three eutectics: native Bi + hedleyite (Bi_7Te_3) at 266 °C (*Okamoto* and *Tanner*, 1990), native Bi + maldonite at 241 °C (*Okamoto* and *Massalski*, 1983) and native Bi + hedleyite + maldonite at 235 °C (*Prince* et al., 1990). Neither these assemblages nor hedleyite or maldonite are, however, present in the associations described here; native Bi is only minor. Instead, all tellurium-bearing phases also contain S and Se (i.e., ingodite, ikunolite, laitakarite); jonassonite is a further S-bearing phase. It is thus appropriate to consider that melting of native Bi took place under sulfidation at the very beginning of the melting episode, with the result that Bi_{melt} reacted with S_2(g) and formed a melt close to BD_{10} composition. Replacement of pyrrhotite by pyrite, observed throughout all samples, indicates that such an increase in sulfidation state was recorded during the shearing episode. The preservation of abundant pyrrhotite relicts within pyrite is evidence for incomplete re-equilibration within the ore.

The presence of Pb in the mineral assemblages, as discussed above, implies that this element must also be incorporated in the melt at an early stage. Reaction of molten Bi with inclusions of galena will be able to provide sufficient Pb and a minimum amount of S. At 400 °C, a narrow field of Bi-melt incorporating only 1 at.% Pb and 6 at.% S is shown in equilibrium with galena on the Bi–Pb–S ternary diagram (e.g., *Craig*, 1967).

On the other hand, melting of any Bi–Pb-sulfosalt present in the vein prior to shearing would form melts with Bi–Pb–S compositions close to the cosalite-dominated assemblages that we describe. Sulfosalt-derived melts, alone or by interaction with molten Bi are thus to be considered as the second scavenger for Au at the temperature range of the shearing event. For example, an association of native Bi + bismuthinite (representing the only eutectic in the Bi–S system) is formed at almost the same temperature at which native Bi melts (270 °C; *Lin* et al., 1990 in *Villars* et al., 1995). Interaction between molten Bi and any bismuthinite derivative, if this was present in the vein prior to shearing, will thus provide Bi-melts with low Pb contents that will result in the BD_{10}-dominated assemblages described here. Formation of two types of melts as discussed above would better explain why there

are two populations of blebs/patches that contain Au, either as native Au or jonassonite or both (Table 2).

Phase separation from the melts

The assemblages obtained at the minimum solvus temperature where two (or three) solids are formed from a liquid in equilibrium with their respective solvus represent eutectics in a given system. Crystallization of a melt formed at temperatures above the eutectic will conclude with the formation of the eutectic assemblage as the end product. The eutectic assemblage is obtained when cooling reaches the eutectic temperature, despite the fact that the initial melt composition may differ from that of the eutectic itself (e.g., *Reed-Hill* and *Abbaschian*, 1991). This is true for compositions on either side of the eutectic and is realized by gradually shifting the melt composition on the solvus curve towards that at the eutectic as the result of partial crystallization of phases situated above this point from the initial melt. This is an important mechanism for Au extraction, especially from melts in which gold is incorporated in only minor amounts (below eutectic concentration), as it appears to be in the Highiş case. On the other hand, the ability to form a melt in a given system is enhanced if structural compatibility between phases will allow extensive solid-solution fields to occur. Exsolution will provide a second mechanism to extract elements incorporated within melts, assuming that immiscibility points are reached along the cooling path(s). The assemblages formed at a eutectic show symplectitic textures if they are rapidly cooled (or quenched); similar textures may also be obtained via exsolution. When the cooling rate is slow, the mineral assemblages will instead display triple joint junctions between the phases formed at eutectic.

Textural evidence in the Highiş occurrence suggests that both types of processes were involved in extraction of Au and Te from the Bi–Pb–S melts. Mutual curvilinear boundaries joined at a triple point are observed between Bi-minerals (e.g., Fig. 7f), suggesting that some of the Bi–Pb–S–Te–(Cu) melts underwent internal phase separation caused by liquid immiscibility before the onset of crystallization. Such triple points, characteristic of formation at equilibrium (the eutectic on a slow cooling path), were also observed for patches including native gold (Fig. 5e, i), although without preservation of the curvilinear boundaries.

The banding observed at the low angle corner between ingodite and cosalite (Fig. 7g, h) and also jonassonite (Fig. 7i) may be interpreted as a 'dissipative' texture that was generated after melt separation within the patches. This type of texture is produced and preserved during crystallization in a steady-state regime if the minerals involved share elements of structural compatibility (*Ortoleva*, 1994). Since melt formation is dependant upon the ability of mineral phases to form a solid-solution at temperatures above their respective solid-state stability temperatures, this presumption allows us to consider the observed banding textures as evidence for a melt in the 5-component system Au–Bi–Pb–S–Te for which there are no experimental data.

The partial liquidus projection (in the range 40 to 100 at.% Bi) within the system Bi–S–Te (*Amadori*, 1918, 1920 in *Villars* et al., 1995) shows that the diagram consists of a two-field melt domain separated by a eutectic line of composition e_2: $l = Bi_2S_3 + Bi_4S_3Te_3$ at temperatures above 260 °C. The importance of eutectic line e_2 is that it will result in this mineral assemblage even though only 15 at.% Te

and 2–3 at.% S can be incorporated within this melt. The observed exsolutions of ingodite, Bi(S,Te), within BD_{10} (Fig. 7b–d) may thus be interpreted as the crystallization products of an analogous melt with a close-to-BD_{10} composition.

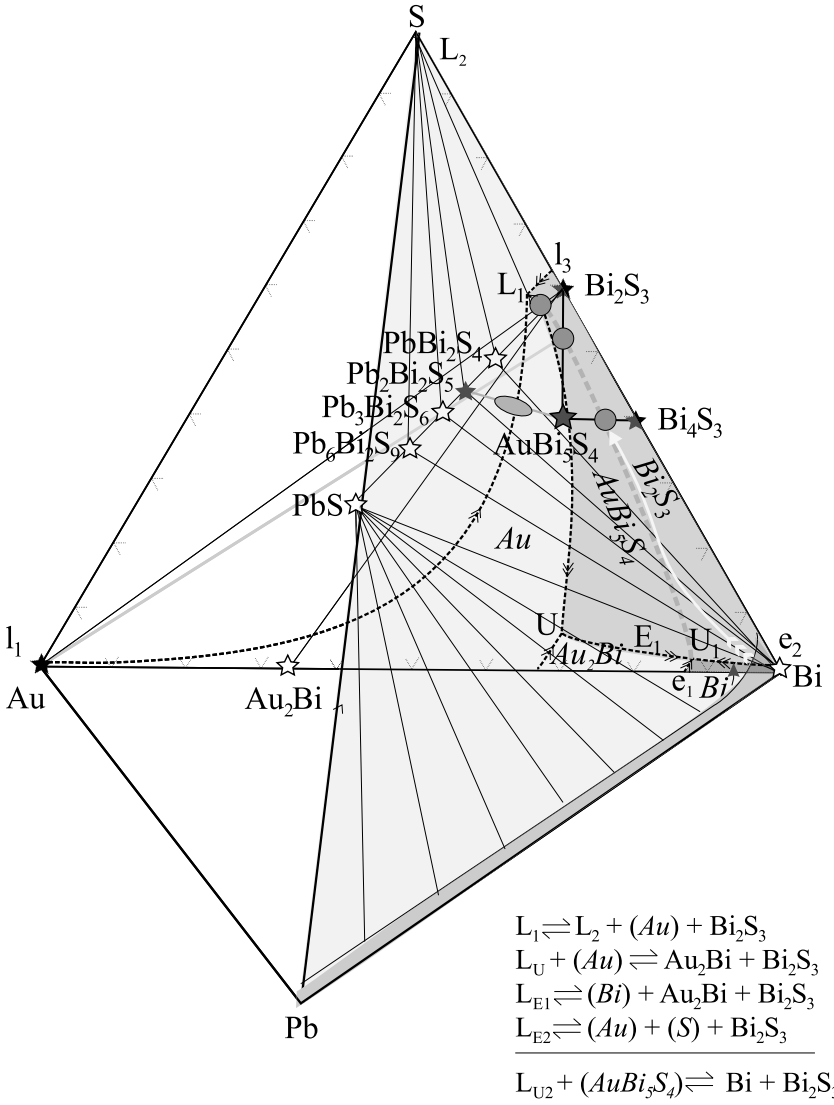

Fig. 11. Diagram illustrating phase relationships in the Au–Pb–Bi–S system. The Au–Bi–S diagram represents the hypothetical projection of liquidus (after *Gather* (1976) cited in *Prince* et al., 1990). Shaded area is the Pb–Bi–S ternary modified after isotherm at 400 °C given by *Craig* (1967). Phases shown by black stars are present in the Highiş samples; other phases – white stars. Solid lines show two-phase assemblages, dashed lines are reaction curves. Bold lines represent our interpretation based on observed assemblages. Melt fields are named in italics. Full circles are the three hypothetical eutectic compositions, i.e., $AuBi_5S_4$–Bi_4S_3, $AuBi_5S_4$–Bi_2S_3, Bi_2S_3–Au; ellipse is the $AuBi_5S_4$–$Pb_2Bi_2S_5$ eutectic. Arrowed white line represents path of melt evolution from native bismuth to bismuthinite, reaching the respective eutectics. The four reactions are from *Gather* (1976) cited in *Prince* et al. (1990); the fifth reaction (below the line) is our interpretation. Double arrows indicate down-temperature paths. $AuBi_5S_4$: jonassonite; Bi_4S_3: ikunolite; Bi_2S_3: bismuthinite; $Pb_2Bi_2S_5$: cosalite

Jonassonite and native gold in the Highiş occurrence: implication for the Au–Bi–(Pb)–S system

There are no experimental data for the system Au–Bi–S, although a hypothetical diagram projecting the liquidus surface has nonetheless been proposed (*Gather,* 1976 in *Prince* et al., 1990; Fig. 11). The predicted assemblage bismuthinite + native gold is observed in many of the blebs (as BD_{10}–Au; Fig. 5h–j) and may be interpreted to represent the binary eutectic (?), positioned at the junction between the solvus line $L_1 = L_2 + (Au) + Bi_2S_3$ and the Au–Bi_2S_3 tie-line, very close to the bismuthinite.

If jonassonite is plotted on this diagram, it is near to the invariant reaction line: $L_U + (Au) = Au_2Bi + Bi_2S_3$ (Fig. 11). The observed associations of this compound with ikunolite on the one hand (Fig. 5g), and BD_{10} (Fig. 5c) on the other, may each be interpreted as representing binary solid eutectic (?) equivalents of a melt located along the respective tie-line in the Au–Bi–S diagram. We can thus further speculate that another reaction line can be considered in this system. This line will link the E_1 liquid line (given by the reaction $L_{E1} \Leftrightarrow (Bi) + Au_2Bi + Bi_2S_3$) from the junction point between liquid Bi and liquid Au_2Bi and the Au–Bi_2S_3 tie-line. We suggest that the reaction along such a line separating two liquid fields would be: $L_{U2} + (AuBi_5S_4) \Leftrightarrow Bi + Bi_2S_3$ (Fig. 11).

The association of jonassonite with cosalite (Fig. 5a, b, d, f) is most complex and implies not only crystallization at equilibrium, but also formation of coherent intergrowths inferring possible crystal-chemical affinities between the two minerals (see above). Such an association can only be assessed in the system Au–Bi–Pb–S, for which there are no available data. Considering the fact that this is one of the most common type of Au-bearing bleb, we can only emphasize that a hypothetical melt with composition $\sim(Pb_2Bi_7)_9S_9$ (arbitrarily chosen to represent the sum of equal amounts of cosalite and the proportions of Bi and S in jonassonite, 'Bi_5S_4') are as efficient in incorporating Au as the melts with composition close to BD_{10}.

How many Au-scavengers?

Even though ingodite is present in some of the blebs that include native gold, the sulfotelluride does not display a direct relationship with native gold (Fig. 7h). Interpretation of relationships between ingodite and jonassonite (Fig. 7i) was given above, implying elements of structural compatibility between these two minerals and host cosalite. The lack of relationships with genetic inferences between ingodite and gold minerals suggests that the presence of Te within the Bi-melts did not enhance Au incorporation within those melts, even though Bi-tellurides can act as good Au scavengers (e.g., *Ciobanu* et al., 2005). The reason for this may be the fact that the scavenging process, in this case, was driven by sulfidized Bi-melts only. Incorporation of Te within these Bi melts, even if possible, does not alone provide an independent Au scavenger. The scavenging potential of a telluride melt is limited by the need for the melt temperature to be above the solvus at the composition of the equivalent telluride. Even though data for the ternary phase ingodite are missing, we can use tsumoite (BiTe) for comparison. The latter has a solvus at temperatures above 500 °C (*Okamoto* and *Tanner*, 1990).

If the composition of a specific bleb is calculated from the formulae of mineral components assuming equal proportions of the component minerals (Table 2), in general, the melts in which the ratio between metals (Au, Bi, Pb) and sulfur (+Te, Se) ≥ 1 are better suited for incorporation of Au. Although these do not represent the real melt compositions, they provide a basis for comparison between the respective assemblages. The above conclusion may suggest that the scavenging efficiency of the melts for Au, although initially supported by sulfidation, diminished as fS_2 attained maximum values, as reflected by blebs where sulfur exceeds total metals.

Gold in Alpine shear-remobilizates from the Highiş Massif

Although a tectonothermal Variscan event was detected within phyllonites from the northern margin of Highiş Massif, this was at 320–300 Ma (*Dallmeyer* et al., 1999), some 40 Ma before the emplacement of the Jernova granitoid (264 Ma; *Pană* et al., 2002). Therefore, since the Şoimuş Ilii vein is formed within the contact aureole of this intrusion, which is part of the igneous core of the Highiş Massif, we interpret the range of shearing-associated processes for the vein as being related to the Alpine overprint at 114–100 Ma (*Dallmeyer* et al., 1999). *Dallmeyer* et al. (1999) recorded temperatures of 100–150 °C within the minerals associated with this event (i.e., much lower than either the ca. 400 °C which we invoke), or the general estimates for Alpine metamorphic conditions given by *Pană* and *Erdmer* (1994), for phyllonites from the margin of the HBSZ, rather than lithologies from the median vein-bearing part.

We conclude that the data presented above indicate formation of Au mineralization in vein remobilizate ores during Alpine penetrative shearing detected throughout the entire HBSZ. This also raises the possibility of the presence of other Au occurrences within the same greenschist belt.

Conclusions

1. The Highiş occurrence contains previously unreported gold mineralization. Gold minerals, of which jonassonite is most abundant, are closely associated with Bi-sulfosalts and -tellurides.
2. The Au–Bi–Te association can be linked to the formation of Bi melts under sulfidation conditions. The Highiş occurrence demonstrates the significant potential role of LMCE as Au scavengers at temperatures as low as 400 °C.
3. The new data for jonassonite should stimulate attempts to ascertain its stability relationships. The presence of jonassonite in Highiş, and other occurrences, illustrates the role that variable sulfidation conditions play in enhancing Au concentration.
4. All evidence points to deposition of the Au–Bi–S–Te assemblages from an internal remobilizate during Alpine shearing in the Early Cretaceous.

Acknowledgements

This study is a contribution to International Geoscience Programme (IGCP) project 486. CLC gratefully acknowledges receipt of an ARC Discovery fellowship. Adelaide Microscopy

Centre is acknowledged for assistance with microanalysis. The reviewers, *Andrew Tomkins* and *Antonia Cepedal*, are thanked for their constructive reviews. Comments from *Paul Spry* greatly assisted us to improve the clarity of the manuscript.

References

Amadori M (1918) Ricerche sul gruppo dei telluri di bismuto. Atti della Accad Naz del Lincei, Classe Scienze Fis, Math. Nat Rend 27: 131–136

Amadori M (1920) Untersuchung über die Gruppe der Wismuttelluride. Z Metallkunde 12: 125–126

Balintoni I (1986) Petrologic and tectonic features of the Highiş-Drocea crystalline massif (Apuseni Mountains). Dari de Seama Inst Geol Geofiz 70–71: 5–21

Bleahu M, Lupu M, Patrulius D, Bordea S, Ştefan A, Panin S (1981) The structure of the Apuseni Mountains. In: Carpatho-Balkan Geological Association, XII Congress, Bucharest, Romania. Guide to Excursion-B3, 103 pp

Brana V (1958) Zăcămintele Metaliifere ale Subsolului Romînesc. Editura Stiinţifica, Bucharest, 261 pp

Chang LLY, Hoda SH (1977) Phase relations in the system $PbS–Cu_2S–Bi_2S_3$ and the stability of galenobismutite. Am Mineral 62: 346–350

Ciobanu CL, Cook NJ, Pring A (2005) Bismuth tellurides as gold scavengers. In: *Mao JW, Bierlein FP* (eds) Mineral deposit research: meeting the global challenge, Springer, Berlin-Heidelberg-New York, pp 1383–1386

Cook NJ, Ciobanu CL, Stanley CJ, Paar W, Sundblad K (2006) Modularity and compositional constraints among Pb–Bi tellurosulphides. Can Mineral 44: (in press)

Craig JR (1967) Phase relations and mineral assemblages in the Ag–Bi–Pb–S system. Mineralium Deposita 1: 278–306

Dallmeyer RD, Pană DI, Neubauer F, Erdmer P (1999) Tectonothermal evolution of the Apuseni Mountains, Romania; resolution of Variscan versus Alpine events with $^{40}Ar/^{39}Ar$ ages. J Geol 107: 329–352

Dimitrescu R (1962) Cercetări geologice in regiunea Şiria. D S Com Geol 45: 75–87

Dimitrescu R (1985) Early Caledonian event in the pre-Alpine metamorphic assemblages of the Romanian Carpathians. Acta Mineral Petrogr Szeged 27: 59–70

Dobosi G, Nagy B (1989) The occurrence of an Au–Bi sulfide in the Nagybörzsöny hydrothermal ore deposit, Northern Hungary. N Jahrb Mineral Monatsh: 8–14

Frost BR, Mavrogenes JA, Tomkins AG (2002) Partial melting of sulfide ore during medium- and high-grade metamorphism. Can Mineral 40: 1–18

Gather B, Blachnik R (1974) Das System Gold-Wismut-Tellur. Z Metallkunde 65: 653–656

Giuşcă D (1957) Observatii asupra mineralizatiilor cuprifere din masivul Highiş. Analele Univ. C.I. Parhon, Bucuresti, ser. Ştiinţele naturii 16: 161–165

Giuşcă D (1962) Observatii asupra formatiunilor cristaline si metamorfismului de contact al granitelor din masivul Highiş. Ed. Academiei, St cerc geol VII 2: 319–327

Giuşcă D (1979) Masivul cristalin al Highişului. Stud şi Cerc Geol, Geofiz, Geogr, Ser Geol 24: 15–43

Giuşcă D, Savu H, Borcoş M (1968) La stratigraphie des schistes cristallines des Monts Apuseni. Rev Roum Geol 12: 143–159

Goldfarb RJ, Groves DI, Gardoll S (2001) Orogenic gold and geologic time: a global synthesis. Ore Geol Rev 18: 1–75

Groves DI, Goldfarb RJ, Gebre-Mariam M, Hagemann SG, Robert F (1998) Orogenic gold deposits: a proposed classification in the context of their crustal distribution and relationship to other gold deposit types. Ore Geol Rev 13: 7–27

Hamasaki S, Murao S, Hoshino K, Watanabe M (1986) Unnamed Au–Bi sulfide from the Tsugahira mine, southern Kyushu, SW Japan. N Jahrb Mineral Monatsh: 416–422

Hoda SN, Chang LLY (1975) Phase relations in the systems PbS–Ag_2S–Sb_2S_3 and PbS–Ag_2S–Bi_2S_3. Amer Mineral 60: 621–633

Horner J, Neubauer F, Paar WH, Hansmann W, Koeppel V, Robl K (1997) Structure, mineralogy, and Pb isotopic composition of the As–Au–Ag deposit Rotgülden, Eastern Alps (Austria): significance for formation of epigenetic ore deposits within metamorphic domes. Mineral Deposita 32: 555–568

Ianovici V, Borcoş M, Bleahu M, Patrulius D, Lupu M, Dimitrescu R, Savu H (1976) Geologia Muntilor Apuseni. Ed. Academiei, Bucuresti, 631 pp

Lin JC, Sharma RC, Chang YA (1990) Bi–S (bismuth-sulfur). In: *Massalski TB, Ohamoto K* (eds) Binary alloy phase diagrams, ASM International, Materials Park, Ohio, pp 783–787

Makovicky E (1989) Modular classification of sulphosalts – current status. Definition and application of homologous series. N Jahrb Mineral Abh 160: 269–297

Marshall B, *Gilligan LB* (1993) Remobilization, syn-tectonic processes and massive sulphide deposits. Ore Geol Rev 8: 39–64

Marshall B, Vokes FM, Larocque ACL (2000) Regional metamorphic remobilization: upgrading and formation of ore deposits. Rev Econ Geol 11: 19–38

Nekrasov IY, Yakovlev YV, Solov'ev LI, Leskova NV (1988) Discovery of gold–bismuth sulfide. Dokl Akad Nauk SSR 299: 438–441

Okamoto H, Massalski TB (1983) Au–Bi (gold–bismuth). In: *Massalski TB* et al. (eds) Binary alloy phase diagrams, vol 1: Ac–Au to Fe–Rh. Ohio, ASM International, Materials Park, Ohio, pp 238–240

Okamoto K, Tanner LE (1990) Bi–Te (bismuth–tellurium). In: *Massalski TB, Ohamoto K* (eds) Binary alloy phase diagrams, ASM International, Materials Park, Ohio, pp 800–801

Ortoleva PJ (1994) Geochemical self-organization. Oxford Monographs on Geology and Geophysics 23, Oxford University Press, Oxford, 411 pp

Oudin E, Jouhari A, Tane TL, Wadjinny A (1988) Observation d'un sulfure d'or-plomb-bismuth $Au(Bi,Pb)_5S_4$ dans une minéralisation du massif du Tichka (Haut-Atlas occidental, Maroc). Principaux Resultats Scientifiques et Techniques du BRGM 1988: 169

Paar WH, Putz H, Roberts AC, Stanley CJ, Culetto FJ (2006) Jonassonite, $Au(Bi,Pb)_5S_4$, a new mineral species from Nagybörzsöny, Hungary. Can Mineral 44: (in press)

Pană D (1998) Petrogenesis and tectonics of the basement rocks of the Apuseni Mountains: significance for the Alpine tectonics of the Carpathian-Pannonian region. PhD. Thesis, University of Alberta, Canada

Pană D, Erdmer P (1994) Alpine crustal shear zones and pre-Alpine basement terranes in the Romanian Carpathians and Apuseni Mountains. Geology 22: 807–810

Pană D, Ricman C (1988) The lower complex of the Păşiuşeni Series – a blastomylonitic shear belt. Rev Roum Géol Géophys Géogr, ser Géol 32: 21–35

Pană DI, Heaman LM, Creaser RA, Erdmer P (2002) Pre-Alpine crust in the Apuseni Mountains, Romania; insights from Sm–Nd and U–Pb data. J Geol 110: 341–354

Pavlova SN, Kotelinikov PE (1988) The form and distribution of silver, bismuth, tellurium, selenium, cobalt and antimony in copper–gold ore deposits of Kasachstan. Izvestia Akad Nauk Kazakh SSR, ser Geol 13–23

Prince A, Raynor GV, Evans DS (1990) Phase diagrams of ternary gold alloys. The Institute of Metals, London, 505 pp

Pring A (1995) Annealing of synthetic hammarite, $Cu_2Pb_2Bi_4S_9$, and the nature of cation-ordering processes in the bismuthinite-aikinite series. Am Mineral 80: 1166–1173

Pring A, Jercher M, Makovicky E (1999) Disorder and compositional variation in the lillianite homologous series. Mineral Mag 63: 917–926

Pring A, Etschmann B (2002) HRTEM observations of structural and chemical modulations in cosalite and its relationship to the lillianite homologues. Mineral Mag 66: 541–458

Reed-Hill RE, Abbaschian R (1991) Physical metallurgy principles, 3rd ed. PWS Publ Co, Boston, 926 pp

Sadykhova SA, Safarov MG, Rustamov PG (1977) Interaction in the Bi_2S_3–PbS system. Russ J Inorg Chem 22: 1537–1539

Salanci B, Moh GH (1969) An experimental study of the pseudobinary join PbS–Bi_2S_3 of the system Pb–Bi–S and its relation to natural lead–bismuth sulfosalts. N Jahrb Mineral Abh 112: 63–95

Savu H, Kräutner F (1972) Harta genetică a substanţelor minerale utile sc. 1:200 000. Notă explicativă pentru foaia 16 Arad. Ed Inst Geol Bucharest, 42 pp

Schneiderhöhn H (1941) Lehrbuch der Erzlagerstättenkunde. Foscher Verlag, Jena, 858 pp

Springer G (1971) The synthetic solid-solution series Bi_2S_3–$BiCuPbS_3$ (bismuthinite-aikinite). N Jahrb Mineral Monatsh: 19–27

Stegman CL (2001) Cobar deposits: still defying classification. SEG Newsletter 44: 1 and 15–26

Tomkins AG, Mavrogenes JA (2002) Mobilization of gold as a polymetallic melt during pelite anatexis at the Challenger gold deposit, South Australia: A metamorphosed Archean deposit. Econ Geol 97: 1249–1271

Tomkins AG, Mavrogenes JA (2003) Generation of metal-rich felsic magmas during crustal anatexis. Geology 31: 765–768

Tomkins AG, Pattison DRM, Zaleski E (2004) The Hemlo gold deposit, Ontario: an example of melting and mobilization of a precious metal-sulfosalt assemblage during amphibolite facies metamorphism and deformation. Econ Geol 99: 1063–1084

Topa D, Makovicky E, Paar WH (2002) Composition ranges and exsolution pairs for the members of the bismuthinite-aikinite series from Felbertal, Austria. Can Mineral 40: 849–869

Vanhanen E (2001) Geology, mineralogy and geochemistry of the Fe–Co–Au–(U) deposits in the Paleoproterozoic Kuusamo Schist Belt, northeastern Finland. Geol Surv Finland Bull 399: 1–229

Villars P, Prince A, Okamoto H, eds. (1995) Handbook of ternary alloy phase diagrams. ASM International, Materials Park, Ohio 10-volume set

Authors' addresses: *C. L. Ciobanu* (corresponding author, e-mail: Cristiana.Ciobanu@adelaide.edu.au; Ciobanu.Cristiana@saugov.sa.gov.au) Department of Earth Sciences, University of Adelaide, North Terrace, Adelaide, SA 5000, Australia and South Australian Museum, North Terrace, Adelaide, SA 5005, Australia, *Nigel J. Cook* (e-mail: nigelc@nhm.uio.no) Natural History Museum, University of Oslo, Postboks 1172, Blindern, N-0318 Oslo, Norway, *Floarea Damian* and *Gheorghe Damian* (e-mail: damgeo@ubm.ro), North University of Baia Mare, RO-4800 Baia Mare, Romania